The CMB Quadrupole depression produced by early fast-roll inflation: MCMC analysis of WMAP and SDSS data.

C. Destri[(a),][*] **H. J. de Vega**[(b,c),][†] **and N. G. Sanchez**[(c)‡]

[(a)] *Dipartimento di Fisica G. Occhialini, Università Milano-Bicocca Piazza della Scienza 3,*
20126 Milano and INFN, sezione di Milano, via Celoria 16, Milano Italia
[(b)] *LPTHE, Laboratoire Associé au CNRS UMR 7589,*
Université Pierre et Marie Curie (Paris VI) et Denis Diderot (Paris VII),
Tour 24, 5 ème. étage, 4, Place Jussieu, 75252 Paris, Cedex 05, France.
[(c)] *Observatoire de Paris, LERMA, Laboratoire Associé au CNRS UMR 8112,*
61, Avenue de l'Observatoire, 75014 Paris, France.
(Dated: June 4, 2008)

Generically, the classical evolution of the inflaton has a brief **fast roll stage** that precedes the slow roll regime. The fast roll stage leads to a purely attractive potential in the wave equations of curvature and tensor perturbations (while the potential is purely repulsive in the slow roll stage). This attractive potential leads to a **depression** of the CMB quadrupole moment for the curvature and B-mode angular power spectra. A single **new** parameter emerges in this way in the early universe model: the comoving wave number k_1 characteristic scale of this attractive potential. This mode k_1 happens to exit the horizon precisely **at the transition** from the fast-roll to the slow-roll stage. The fast-roll stage dynamically modifies the initial power spectrum by a transfer function $D(k)$. We compute $D(k)$ by solving the inflaton evolution equations. $D(k)$ effectively suppresses the primordial power for $k < k_1$ and posseses the scaling property $D(k) = \Psi(k/k_1)$ where $\Psi(x)$ is an universal function. We perform a MCMC analysis of the WMAP and SDSS data including the fast-roll stage and find the value $k_1 = 0.266 \ \mathrm{Gpc}^{-1}$. The quadrupole mode $k_Q = 0.242 \ \mathrm{Gpc}^{-1}$ exits the horizon earlier than k_1, about one-tenth of an efold before the end of fast-roll. We compare the fast-roll fit with a fit without fast roll but including a sharp lower cutoff on the primordial power. Fast-roll provides a slightly better fit than a sharp cutoff for the TT, TE and EE modes. Moreover, our fits provide **non-zero** lower bounds for r, while the values of the other cosmological parameters are essentially those of the pure ΛCDM model. We display the real space two point $C^{TT}(\theta)$ correlator. The fact that k_Q exits the horizon before the slow-roll stage implies an **upper** bound in the total number of efolds N_{tot} during inflation. Combining this with estimates during the radiation dominated era we obtain $N_{tot} \sim 66$, with the bounds $62 < N_{tot} < 82$. We repeated the same analysis with the WMAP-5, ACBAR-2007 and SDSS data confirming the overall picture.

Contents

[*]Electronic address: Claudio.Destri@mib.infn.it
[†]Electronic address: devega@lpthe.jussieu.fr
[‡]Electronic address: Norma.Sanchez@obspm.fr

I. INTRODUCTION AND RESULTS

The Standard (Concordance) Model of the Universe explains today a wide set of cosmological and astronomical measurements performed over a large variety of wave-lenghts and observation tools: large and small angular scale CMB observations, light elements abundances, large scale structure observations (LSS) and properties of galaxy clusters, Hubble Space Telescope measurements on the Hubble constant, supernova luminosity/distance relations (acceleration of the today universe expansion), and other measurements. The concordance of these data imply that our universe is spatially flat, with gravity and cosmological perturbations described by Einstein General Relativity theory. WMAP data give a strong support to the Standard Model of the Universe.

Inflation was introduced to solve several outstanding problems of the standard Big Bang model [1] and has now become an important part of the Standard Model of the Universe. At the same time, it provides a natural mechanism for the generation of scalar density fluctuations that seed large scale structure, thus explaining the origin of the temperature anisotropies in the cosmic microwave background (CMB), as well as that of tensor perturbations (primordial gravitational waves) [2, 16].

The horizon and flatness problems are solved provided the universe expands for more than 62 efolds during inflation. This is achieved within slow-roll inflation where the inflaton potential is fairly flat.

Although there are no statistically significant departures from the slow roll inflationary scenario at small angular scales ($l \gtrsim 100$), the WMAP data again confirms the surprinsingly low quadrupoles C_2^{TT} and C_2^{TE} [8]-[9] and suggests that it cannot be completely explained by galactic foreground contamination. The low value of the quadrupole has been an intriguing feature on large angular scales since first observed by COBE/DMR [4], and confirmed by the WMAP data [8]-[9].

In order to asses the relevance of the observed quadrupole suppression in the ΛCDM model, we determine in the best fit ΛCDM model the probability to observe the quadrupole 20% below the theoretical mean value. This probability turns out to be only ~ 0.06. This small probability supports the necessity for a cosmological explanation of the quadrupole depression beyond the ΛCDM model.

Generically, the classical evolution of the inflaton has a brief **fast roll stage** that precedes the slow roll regime. The fast roll stage leads to a purely attractive potential in the wave equations of curvature and tensor perturbations. Such potential is a *generic* feature of this brief *fast roll* stage that merges smoothly with slow roll inflation. This stage is a consequence of generic initial conditions *for the classical inflaton dynamics* in which the kinetic and potential energy of the inflaton are of the same order, namely, the energy scale of slow roll inflation. During the early fast roll stage the inflaton evolves rapidly during a brief period, but slows down by the cosmological expansion settling in the slow roll stage in which the kinetic energy of the inflaton is much smaller than its potential energy.

As shown in ref. [6, 7] the attractive potential in the wave equations of curvature and tensor perturbations during the fast-roll stage leads to a **suppression** of the quadrupole moment for CMB and B-mode angular power spectra. Both scalar and tensor low multipoles are suppressed. However, the potential for tensor perturbations is about an order of magnitude smaller than the one for scalar fluctuations and hence the suppression of low ℓ tensor perturbations is much less significative [6, 7].

The observation of a low quadrupole [4, 8, 9] and the surprising alignment of quadrupole and octupole [10, 11] sparked many different proposals for their explanation [12].

The fast-roll explanation of the quadrupole does not require to introduce new physics neither modifications of the slow-roll inflationary models. The only new feature is that the quadrupole mode should exit the horizon during the generic fast-roll stage that precedes slow-roll inflation.

A single **new** parameter emerges dynamically due to the fast-roll stage: the comoving wave number k_1, characteristic scale of the attractive potential felt by the fluctuations during fast-roll. The fast-roll stage modifies the initial power spectrum by a transfer function $D(k)$ that we compute solving the classical inflaton evolution equations [see fig. 3]. $D(k)$ effectively suppresses the primordial power for $k < k_1$ and posseses the scaling property $D(k) = \Psi(k/k_1)$ where $\Psi(x)$ is an universal function. $D(k)$ has a main peak around $k_M \simeq 1.9\ k_1$ and oscillates around zero with decreasing amplitude as a function of k for $k > k_M$. $D(k)$ vanishes asymptotically for large k, as expected.

We report here the results of a MCMC analysis of the WMAP-3, small–scale CMB and SDSS data including the fast-roll stage and find the value $k_1 = 0.266$ Gpc^{-1}. This mode k_1 happens to exit the horizon precisely at the transition from the fast-roll to the slow-roll stage. The quadrupole mode $k_Q = 0.242$ Gpc^{-1} exits the horizon **during** the fast-roll stage approximately **1/10 of an efold earlier** than k_1. We compare the fast-roll fit with a fit without

fast roll but including a sharp lower cutoff on the primordial power. Fast-roll provides a slightly better fit than a sharp cutoff for the C_ℓ^{TT}, C_ℓ^{TE} and C_ℓ^{EE} coefficients. Besides reproducing the quadrupole depression, the fast roll fit accounts for the oscillations of the lower multipole data.

We analyze with MCMC and compare three classes of cosmological models:

- The usual slow-roll ΛCDM, the ΛCDM+r and the ΛCDM+r on C_{BNI} models. BNI stands for *Binomial New Inflation*. In this last model we **enforce** the theoretical functional relation (denoted C_{BNI}) between n_s and r valid in BNI.(We call ΛCDM+r on C_{BNI} the usual ΛCDM+r model constrained on the curve C_{BNI}).

- The slow-roll ΛCDM on C_{BNI} model with a sharp cut for $k < k_1$.

- The ΛCDM on C_{BNI} model including both fast and slow-roll stages.

The MCMC analysis of the WMAP and SDSS data favours a double-well, spontaneously broken symmetric potential for the inflaton in new inflation [15]

$$V(\varphi) = \frac{\lambda}{4} \left(\varphi^2 - \frac{m^2}{\lambda} \right)^2 .$$

The quartic coupling in the effective theory of inflation [5] is given by

$$\lambda = \frac{y}{8\,N} \left(\frac{M}{M_{Pl}} \right)^4 \sim 10^{-12} .$$

Here $N \sim 60$ is the number of efolds since the cosmologically relevant modes exit the horizon till the end of inflation and $M_{Pl} = 2.4 \times 10^{18}$ GeV is the Planck mass. MCMC yields for the dimensionless quartic coupling $y \simeq 1.32$ and

$$M = 0.57 \times 10^{16} \text{ GeV} \quad , \quad m = 1.34 \times 10^{13} \text{ GeV}$$

for the inflation energy scale M and the inflaton mass scale m, respectively.

We modified the *CosmoMC* code introducing the fast roll transfer function $D_{\mathcal{R}}(k)$ in the primordial power spectrum according to eq. (3.31).

We repeated the same analysis with the WMAP-5, ACBAR-2007 and SDSS data, this time setting $N = 60$, with no statistically significant change.

Our fits imposing C_{BNI} predict **non-zero** lower bounds on r: at 95% CL, we find that $r > 0.023$ when no cutoff is introduced, while $r > 0.018$ when either the sharp cutoff or the fastroll $D(k)$ are introduced. The best fit values of the other cosmological parameters remain practically unchanged as compared to ΛCDM. Similarly their marginalized probability distributions are almost unchanged, with the natural exception of n_s, which in BNI has a theoretical upper limit [see eq. (5.6)].

We observe that the oscillatory form of the fastroll transfer function $D_{\mathcal{R}}(k)$, by **depressing as well as enhancing** the primordial power spectrum at long wavelengths, leads also to new superimposed **oscillatory corrections** on the low multipoles. As far as fitting to current data is concerned, such corrections are more effective than the pure reduction caused by a sharp cutoff. The fast-roll oscillations yield better gains in likelihood than the sharpcut case.

We display the best fit for the C_ℓ^{TT}, C_ℓ^{TE} and C_ℓ^{EE} multipoles compared to the experimental data at low ℓ. One can observe that for $\ell = 2$ and $\ell = 3$ fast-roll and sharpcut models yield rather similar results (and better than the ΛCDM+r model) while for $\ell = 4$ fast-roll produces for C_ℓ^{TE} a value closer to WMAP-3 data than sharpcut. For C_ℓ^{EE} both fastroll and sharpcut models produce a depression of the low multipoles including the EE quadrupole.

We summarize in the Appendix the numerical code used by us in the simulations.

We display the real space two point TT-correlator $C^{TT}(\theta)$ for purely slow-roll ΛCDM, sharpcut and fast-roll ΛCDM models. The purely slow roll ΛCDM correlator differs from the two others only for large angles $\theta \gtrsim 1$. Since all l-modes besides the lowest ones are practically identical in the three cases, this shows how important are the low multipoles in the large angle correlations.

We get the following picture of the inflationary universe explaining the quadrupole suppression from the effective (Ginsburg-Landau) theory of inflation combined with MCMC simulations of CMB+LSS data. A fast-roll stage lasting about one efold is followed by a slow-roll stage lasting ~ 65 efolds. We have the radiation dominated era after these $\sim 65 + 1 = 66$ efolds of inflation. The quadrupole modes exit the horizon during the fast-roll stage about 0.4 of an

efold after the beginning of inflation and is therefore **suppressed** compared with the modes exiting later the horizon during the slow-roll stage.

The fast-roll stage explains the quadrupole suppression and **fixes the total number of efolds** of inflation. The fact that the quadrupole mode k_Q exits the horizon before the slow-roll stage implies an **upper** bound in the total number of efolds N_{tot} during inflation. Combining this with estimates during the radiation dominated era we obtain $N > 56$, $N_{tot} \sim 66$, the upper bound $N_{tot} < 82$ and the lower bound $N_{tot} > 62$.

Our MCMC simulations give good fits for $N = 50$ and $N = 60$. The bound $N > 56$ therefore favours $N \sim 60$ which implies $N_{tot} \sim 66$ and $H \sim 3 \times 10^{10}$ GeV by the end of inflation.

Changing N from 50 to 60 does not affect significantly the MCMC fits we present in this paper. This is partially due to the fact that a change on y can partially compensate a change on N. More importantly, a 20% change in N may affect the fit of k_1 by a similar amount, leaving unchanged its scale, which is of the order of the inverse Hubble scale.

Another **hint** to increase N above 50 comes from WMAP-5 that gives a larger n_s value and using the theoretical upper limit for n_s [14, 15]: $n_s < 1 - \frac{1.9236...}{N}$, which gives $n_s < 0.9679...$ for $N = 60$. This value is compatible with the n_s value from WMAP5+BAO+SN and no running [9].

II.   THE EFFECTIVE THEORY OF INFLATION. FAST AND SLOW ROLL REGIMES.

The inflaton potential $V(\varphi)$ must be a slowly varying function of φ in order to permit a slow-roll solution for the inflaton field which guarantees a large enough total number of efolds $\gtrsim 62$. Such value is necessary to solve the horizon, flatness and entropy problems.

As discussed in ref. [5], the inflaton potential should have the universal form

$$V(\varphi) = N\, M^4\, w(\chi) , \qquad (2.1)$$

where χ is a dimensionless, slowly varying field

$$\chi = \frac{\varphi}{\sqrt{N}\, M_{Pl}} , \qquad (2.2)$$

and M is the energy scale of inflation, $N \sim 60$ is the number of efolds since the cosmologically relevant modes exit the horizon till the end of inflation.

The energy scale M of inflation is determined by the amplitude of the observed CMB anisotropy, which implies $M \sim 0.7 \times 10^{16}$ GeV. That is, $M \ll M_{Pl}$, which ensures the consistency of the effective theory of inflation.

The dynamics of the rescaled field χ exhibits the slow time evolution in terms of the *stretched* dimensionless time variable,

$$\tau = \frac{t\, M^2}{M_{Pl}\, \sqrt{N}} \quad , \quad \mathcal{H} \equiv \frac{H\, M_{Pl}}{\sqrt{N}\, M^2} = \mathcal{O}(1) . \qquad (2.3)$$

The rescaled variables χ and τ change slowly with time. A large change in the field amplitude φ results in a small change in the χ amplitude, a change in $\varphi \sim M_{Pl}$ results in a χ change $\sim 1/\sqrt{N}$. The form of the potential, eq.(2.1), the rescaled dimensionless inflaton field eq.(2.2) and the time variable τ make **manifest** the slow-roll expansion as a consistent systematic expansion in powers of $1/N$ [5].

We can choose $|w''(0)| = 1$ without loosing generality. Then, the inflaton mass scale at zero field is given by a see-saw formula

$$m^2 = |V''(\varphi = 0)| = \frac{M^4}{M_{Pl}^2} \quad , \quad M \sim 0.7 \times 10^{16}\, \text{GeV} \quad , \quad m = \frac{M^2}{M_{Pl}} \sim 2.0 \times 10^{13}\, \text{GeV} . \qquad (2.4)$$

The Hubble parameter when the cosmologically relevant modes exit the horizon is given by

$$H = \sqrt{N}\, m\, \mathcal{H} \sim 5\, m \sim 1.0 \times 10^{14}\, \text{GeV} , \qquad (2.5)$$

where $\mathcal{H} \sim 1$. As a result, $m \ll M$ and $H \ll M_{Pl}$.

The energy density and the pressure in terms of the dimensionless rescaled field χ and the slow time variable τ take the form,

$$\frac{\rho}{N\,M^4} = \frac{1}{2\,N}\left(\frac{d\chi}{d\tau}\right)^2 + w(\chi) \quad , \quad \frac{p}{N\,M^4} = \frac{1}{2\,N}\left(\frac{d\chi}{d\tau}\right)^2 - w(\chi) \,. \tag{2.6}$$

The equations of motion in the same dimensionless variables become

$$\mathcal{H}^2(\tau) = \frac{1}{3}\left[\frac{1}{2\,N}\left(\frac{d\chi}{d\tau}\right)^2 + w(\chi)\right] \quad,$$

$$\frac{1}{N}\frac{d^2\chi}{d\tau^2} + 3\,\mathcal{H}\,\frac{d\chi}{d\tau} + w'(\chi) = 0 \quad. \tag{2.7}$$

The slow-roll approximation follows by neglecting the $\frac{1}{N}$ terms in eqs.(2.7). Both $w(\chi)$ and $\mathcal{H}(\tau)$ are of order N^0 for large N. Both equations make manifest the slow roll expansion as an expansion in $1/N$.

The number of e-folds $N[\chi]$ since the field χ exits the horizon till the end of inflation (where χ takes the value χ_{end}) can be computed in close form from eqs. (2.7) in the slow-roll approximation (that is, neglecting $1/N$ corrections):

$$\frac{N[\chi]}{N} = -\int_\chi^{\chi_{end}} \frac{w(\chi)}{w'(\chi)}\,d\chi \leqslant 1 \,, \tag{2.8}$$

where we choose $N = N[\chi]$. Therefore, eq.(2.8) determines χ at horizon exit as a function of the couplings in the inflaton potential $w(\chi)$:

$$-\int_\chi^{\chi_{end}} \frac{w(\chi)}{w'(\chi)}\,d\chi = 1 \,. \tag{2.9}$$

Inflation ends after a finite number of efolds provided

$$w(\chi_{end}) = w'(\chi_{end}) = 0 \,. \tag{2.10}$$

So, this condition is enforced in the inflationary potentials.

There are two *generic* inflationary regimes: slow-roll and fast-roll depending on whether [7]

$$\frac{1}{2\,N}\left(\frac{d\chi}{d\tau}\right)^2 \ll w(\chi) \quad : \quad \text{slow} - \text{roll regime}$$

$$\frac{1}{2\,N}\left(\frac{d\chi}{d\tau}\right)^2 \sim w(\chi) \quad : \quad \text{fast} - \text{roll regime} \,. \tag{2.11}$$

Both regimes appear in **all** inflationary models in the class eq.(2.1). Fast-roll clearly corresponds to generic initial conditions for the inflaton field. The fast-roll stage turns to be very short and is generically followed by the slow-roll stage [7].

For the quartic degree potentials $V(\varphi)$, the main two families are:

(a) discrete symmetry ($\varphi \to -\varphi$) breaking potentials (so-called new, or small-field, inflation)

$$V(\varphi) = \frac{\lambda}{4}\left(\varphi^2 - \frac{m^2}{\lambda}\right)^2 = -\frac{m^2}{2}\,\varphi^2 + \frac{\lambda}{4}\,\varphi^4 + \frac{m^4}{4\,\lambda} \,; \tag{2.12}$$

(b) unbroken symmetry potentials (chaotic, or large-field, inflation),

$$V(\varphi) = +\frac{m^2}{2}\,\varphi^2 + \frac{\lambda}{4}\,\varphi^4 \,. \tag{2.13}$$

The corresponding dimensionless potentials $w(\chi)$ take the form

$$w(\chi) = \frac{y}{32}\left(\chi^2 - \frac{8}{y}\right)^2 = -\frac{1}{2}\,\chi^2 + \frac{y}{32}\,\chi^4 + \frac{2}{y} \qquad \text{for new inflation} \tag{2.14}$$

and

$$w(\chi) = \frac{1}{2}\,\chi^2 + \frac{y}{32}\,\chi^4 \qquad \text{for chaotic inflation} \tag{2.15}$$

where the coupling y is of **order one** and

$$\lambda = \frac{y}{8\,N}\left(\frac{M}{M_{Pl}}\right)^4 \sim 10^{-12} \quad .$$

In new inflation the inflaton starts near the local maximum $\chi = 0$ and keeps rolling down the potential hill till it reaches the absolute minimum $\chi = \sqrt{\frac{8}{y}}$. In general, the initial kinetic energy may be of the same order of magnitude as the initial potential energy of the inflaton which defines fast-roll inflation. That is, in general the initial states are not slow-roll.

By numerically solving eqs. (2.7) we find that the fast-roll initial stage of the inflaton becomes very soon a slow-roll stage [7]. This is a general property and implies that the slow-roll regime is an atractor for this dynamical system [3]. We see a de Sitter-like expansion during the slow-roll stage $\tau \lesssim 3$ during which the Hubble parameter decreases slowly and monotonically.

An initial state for the *inflaton* (inflaton classical dynamics) with approximate *equipartition* between kinetic and potential energies is a more *general* initialization of cosmological dynamics in the effective field theory than slow roll which requires that the inflaton kinetic energy is much smaller than its potential energy. The most *generic* initialization of the inflaton dynamics in the effective field theory leads to a *fast roll* stage followed by slow roll inflation [7].

The total number of efolds of inflation is determined by the initial conditions for the inflaton field: $\chi(0) \sim \dot\chi(0) = \mathcal{O}(1)$. Varying these initial conditions the total number of efolds of inflation sweeps a wide range of efold values showing the flexibility of the inflationary model.

We have carried out analogous numerical studies in scenarios of chaotic inflation with similar results: if the initial kinetic energy of the inflaton is of the same order as the potential energy, a *fast roll* stage is *always* present. The evolution of the potentials $\mathcal{V}_{\mathcal{R}}(\eta)$ and $\mathcal{V}_T(\eta)$ felt by the curvature and tensor perturbations are similar to those for new inflation and they are always *attractive* during the fast roll stage (see below).
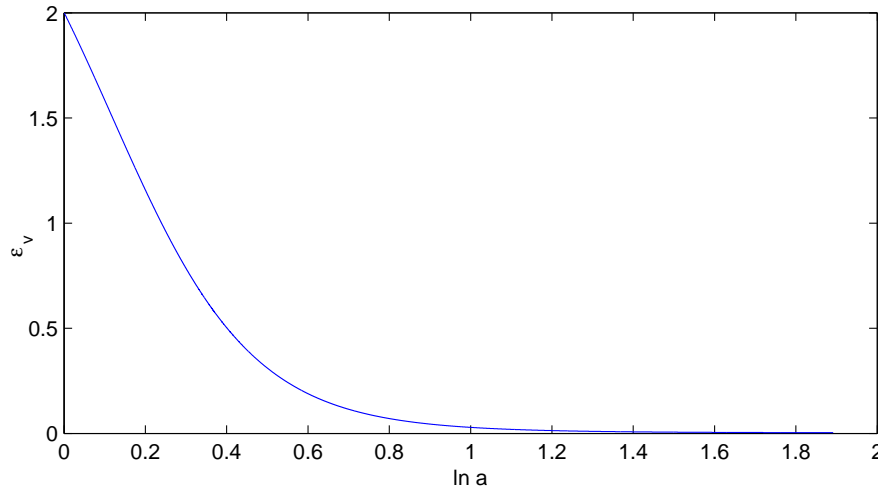

FIG. 1: We plot here ϵ_v vs. $\ln a$ during the fast roll stage and the beginning of slow-roll for new inflation with $y = 1.322$. We define as the end of fast-roll the point where $\epsilon_v = \frac{1}{N} = 0.02$. This gives here $\ln a_F = 1.091$. Namely, fast-roll ends one efold after the beginning of inflation.

III. THE EFFECT OF FAST-ROLL ON THE INFLATIONARY FLUCTUATIONS.

The inflationary scenario features scalar curvature fluctuations determined by a gauge invariant combination of the inflaton field and metric fluctuations. They also feature tensor fluctuations (gravitational waves).

It is convenient to introduce the gauge invariant potential [2],

$$u(\boldsymbol{x}, t) = -z\,\mathcal{R}(\boldsymbol{x}, t)\,, \tag{3.1}$$

where $\mathcal{R}(\boldsymbol{x}, t)$ stands for the gauge invariant curvature perturbation of the comoving hypersurfaces and

$$z \equiv a(t)\,\frac{\dot{\varphi}}{H}\,. \tag{3.2}$$

The gauge invariant curvature field $u(\boldsymbol{x}, t)$ expanded in terms of conformal time mode functions and creation and annihilation operators take the form [2]

$$u(\boldsymbol{x}, \eta) = \int \frac{d^3 k}{(2\,\pi)^{\frac{3}{2}}} \left[\alpha_{\mathcal{R}}(\boldsymbol{k})\,S_{\mathcal{R}}(k; \eta)\,e^{i\boldsymbol{k}\cdot\boldsymbol{x}} + \alpha_{\mathcal{R}}^{\dagger}(\boldsymbol{k})\,S_{\mathcal{R}}^{*}(k; \eta)\,e^{-i\boldsymbol{k}\cdot\boldsymbol{x}}\right]\,, \tag{3.3}$$

where the operators obey canonical commutation relations

$$\left[\alpha_{\mathcal{R}}(\boldsymbol{k}),\ \alpha_{\mathcal{R}}^{\dagger}(\boldsymbol{k}')\right] = \delta^{(3)}(\boldsymbol{k} - \boldsymbol{k}')\,.$$

The vacuum state is annihilated by the operators $\alpha_{\mathcal{R}}(k)$ and the mode functions obey the equations of motion [2],

$$\left[\frac{d^2}{d\eta^2} + k^2 - \frac{1}{z}\frac{d^2 z}{d\eta^2}\right] S_{\mathcal{R}}(k; \eta) = 0\,. \tag{3.4}$$

Here η stands for the conformal time

$$\eta = \int \frac{dt}{a(t)}\,. \tag{3.5}$$

Eq. (3.4) is a Schrödinger-type differential equation in the variable η. The potential felt by the fluctuations

$$W_{\mathcal{R}}(\eta) \equiv \frac{1}{z}\,\frac{d^2 z}{d\eta^2} \tag{3.6}$$

can be expressed in terms of the inflaton potential and its derivatives. From eqs.(3.2) and (3.6) and using the inflation equations of motion (2.7), the potential $W_{\mathcal{R}}(\eta)$ can be written as [7]

$$W_{\mathcal{R}}(\eta) = a^2(\eta)\,H^2(\eta)\left[2 - 7\,\epsilon_v + 2\,\epsilon_v^2 - \frac{\sqrt{8\,\epsilon_v}\,V'}{M_{Pl}\,H^2} - \eta_v(3 - \epsilon_v)\right]\,, \tag{3.7}$$

where we take for the sign of the square root $\sqrt{\epsilon_v}$ the sign of $\dot{\varphi}$ and

$$\epsilon_v \equiv \frac{1}{2\,M_{Pl}^2}\,\frac{\dot{\varphi}^2}{H^2}\quad,\quad \eta_v \equiv M_{Pl}^2\,\frac{V''(\varphi)}{V(\varphi)}\,. \tag{3.8}$$

ϵ_v and η_v are the known slow-roll parameters [2]. Notice that eqs. (3.7)-(3.8) are **exact** (no slow-roll approximation).

In terms of the dimensionless variables eqs.(2.1)-(2.3) we obtain for the potential $W_{\mathcal{R}}(\eta)$,

$$W_{\mathcal{R}}(\eta) = a^2(\eta)\,\mathcal{H}^2\,m^2\,N\left[2 - 7\,\epsilon_v + 2\,\epsilon_v^2 - \sqrt{\frac{8\,\epsilon_v}{N}}\,\frac{w'}{\mathcal{H}^2} - \eta_v(3 - \epsilon_v)\right]\,, \tag{3.9}$$

while the parameters ϵ_v and η_v take the form

$$\epsilon_v = \frac{1}{2\,N}\,\frac{1}{\mathcal{H}^2}\left(\frac{d\chi}{d\tau}\right)^2\quad,\quad \eta_v = \frac{1}{N}\,\frac{w''(\chi)}{w(\chi)}\,. \tag{3.10}$$

In the slow-roll regime they can be approximated as

$$\epsilon_v = \frac{1}{2\,N}\left[\frac{w'(\chi)}{w(\chi)}\right]^2 + \mathcal{O}\left(\frac{1}{N^2}\right) = \mathcal{O}\left(\frac{1}{N}\right)\quad,\quad \eta_v = \frac{1}{N}\,\frac{w''(\chi)}{w(\chi)} = \mathcal{O}\left(\frac{1}{N}\right)\,. \tag{3.11}$$

We explicitly see that the parameters ϵ_v and η_v are suppressed by powers of $1/N$ in the slow-roll regime. This result is valid for **all** models in the class defined by eq.(2.1) regardless of the precise form of $w(\chi)$.

Tensor perturbations (gravitational waves) are gauge invariant. The corresponding quantum fields (gravitons) are written as

$$h_j^i(\boldsymbol{x}, \eta) = \frac{2}{a(\eta)\, M_{Pl}} \sum_{\lambda = \times, +} \int \frac{d^3 k}{(2\,\pi)^{\frac{3}{2}}} \; \epsilon_j^i(\lambda, \boldsymbol{k}) \left[e^{i\boldsymbol{k}\cdot\boldsymbol{x}} \; a_{\lambda, \boldsymbol{k}} \; S_T(k, \eta) + e^{-i\boldsymbol{k}\cdot\boldsymbol{x}} \; a_{\lambda, \boldsymbol{k}}^\dagger \; S_T^*(k, \eta) \right] \;, \qquad (3.12)$$

where λ labels the two standard transverse and traceless polarizations $\times$ and $+$. The operators $\alpha_{\lambda, \boldsymbol{k}}$, $\alpha_{\lambda, \boldsymbol{k}}^\dagger$ obey canonical commutation relations, and $\epsilon_{ij}(\lambda, \boldsymbol{k})$ are the two independent symmetric and traceless-transverse tensors constructed from the two independent polarization vectors transverse to $\boldsymbol{k}$, chosen to be real and normalized such that $\epsilon_j^i(\lambda, \boldsymbol{k})\, \epsilon_k^j(\lambda', \boldsymbol{k}) = \delta_k^i\, \delta_{\lambda, \lambda'}$.

The mode functions $S_T(k; \eta)$ obey the differential equation [2, 6, 7]

$$S_T^{''}(k; \eta) + \left[k^2 - \frac{a''(\eta)}{a(\eta)} \right] S_T(k; \eta) = 0 \;. \qquad (3.13)$$

That is, for both scalar curvature and tensor equations we have the equation

$$\left[\frac{d^2}{d\eta^2} + k^2 - W(\eta) \right] S(k; \eta) = 0 \;. \qquad (3.14)$$

where for scalar curvature perturbations $W_{\mathcal{R}}(\eta)$ is given by eq.(3.6) and for tensor perturbations $W_T(\eta)$ is

$$W_T(\eta) = \frac{a''(\eta)}{a(\eta)} \;.$$

It is convenient to explicitly separate the behavior of $W(\eta)$ during the slow roll stage by writing

$$W(\eta) = \mathcal{V}(\eta) + \frac{\nu^2 - \frac{1}{4}}{\eta^2} \;, \qquad (3.15)$$

where the potential $\mathcal{V}(\eta)$ is the fast-roll part and,

$$\nu = \begin{cases} \nu_{\mathcal{R}} = \frac{3}{2} + 3\,\epsilon_v - \eta_v + \mathcal{O}\left(\frac{1}{N^2}\right) & \text{for curvature perturbations} \\[2mm] \nu_T = \frac{3}{2} + \epsilon_v + \mathcal{O}\left(\frac{1}{N^2}\right) & \text{for tensor perturbations} \;. \end{cases} \qquad (3.16)$$

ϵ_v and η_v are given by eqs.(3.8),(3.10).

The potential $\mathcal{V}(\eta)$ is localized in the fast roll stage *prior* to slow roll (during which cosmologically relevant modes cross out of the Hubble radius), $\mathcal{V}(\eta)$ vanishes during slow-roll. In terms of the potential $\mathcal{V}(\eta)$ the equations for the quantum fluctuations read,

$$\left[\frac{d^2}{d\eta^2} + k^2 - \frac{\nu^2 - \frac{1}{4}}{\eta^2} - \mathcal{V}(\eta) \right] S(k; \eta) = 0 \;. \qquad (3.17)$$

A. The Fluctuations during the slow-roll stage

The slow roll dynamics acts through the term

$$\frac{\nu^2 - 1/4}{\eta^2}$$

which is a *repulsive* centrifugal barrier.

During the slow roll stage $\mathcal{V}(\eta)$ is negligeable and the mode equations simplify to

$$\left[\frac{d^2}{d\eta^2} + k^2 - \frac{\nu^2 - \frac{1}{4}}{\eta^2}\right] S_{sr}(k, \eta) = 0 .$$
(3.18)

To leading order in slow roll, ν is constant and for general initial conditions the solution of eq.(3.18) is,

$$S_{sr}(k; \eta) = A(k)\, g_\nu(k; \eta) + B(k)\, [g_\nu(k; \eta)]^* ,$$
(3.19)

where

$$g_\nu(k; \eta) = \frac{1}{2}\, i^{\nu + \frac{1}{2}}\, \sqrt{-\pi\eta}\, H_\nu^{(1)}(-k\eta) ,$$
(3.20)

$H_\nu^{(1)}(z)$ are Hankel functions. These solutions are normalized so that their Wronskian is given by

$$W[g_\nu(k; \eta), g_\nu^*(k; \eta)] = g_\nu'(k; \eta)\, g_\nu^*(k; \eta) - g_\nu(k; \eta)\, [g_\nu'(k; \eta)]^* = -i .$$
(3.21)

The mode functions and coefficients $A(k)$, $B(k)$ will feature a subscript index $\mathcal{R}$, T, for curvature or tensor perturbations, respectively.

For wavevectors deep inside the Hubble radius $|k\eta| \gg 1$, the mode functions have the asymptotic behavior

$$g_\nu(k; \eta) \overset{\eta\to-\infty}{=} \frac{1}{\sqrt{2k}}\, e^{-ik\eta} ,$$
(3.22)

while for $\eta \to 0^-$ the mode functions behave as:

$$g_\nu(k; \eta) \overset{\eta\to 0^-}{=} \frac{\Gamma(\nu)}{\sqrt{2\pi k}}\left(\frac{2}{ik\eta}\right)^{\nu - \frac{1}{2}} .$$
(3.23)

In particular, in the scale invariant case $\nu = \frac{3}{2}$ which is the leading order in the slow roll expansion, the mode functions eqs.(3.20) simplify to

$$g_{\frac{3}{2}}(k; \eta) = \frac{e^{-ik\eta}}{\sqrt{2k}}\left[1 - \frac{i}{k\eta}\right] .$$
(3.24)

B.   The Fluctuations during the earlier fast-roll stage

The mode equation (3.17) can be written as an integral equation. We choose as initial condition the usual Bunch-Davies asymptotic condition

$$S(k; \eta \to -\infty) = g_\nu(k; \eta \to -\infty) = \frac{e^{-ik\eta}}{\sqrt{2k}} .$$
(3.25)

We formally consider here inflation and the conformal time starting at $\eta = -\infty$. However, it is natural to consider that the inflationary evolution of the universe starts at some negative value $\eta_i < \bar{\eta}$, where $\bar{\eta}$ is the conformal time when fast roll ends and slow roll begins.

The mode equation (3.17) can be written as an integral equation including the Bunch-Davies initial condition eq.(3.25),

$$S(k; \eta) = g_\nu(k; \eta) + i\, g_\nu(k; \eta) \int_{-\infty}^{\eta} g_\nu^*(k; \eta')\, \mathcal{V}(\eta')\, S(k; \eta')\, d\eta' - i\, g_\nu^*(k; \eta) \int_{-\infty}^{\eta} g_\nu(k; \eta')\, \mathcal{V}(\eta')\, S(k; \eta')\, d\eta' .$$
(3.26)

where for simplicity we set $\eta_i = -\infty$.

Since $\mathcal{V}(\eta)$ vanishes for $\eta > \bar{\eta}$, the mode functions $S(k; \eta)$ for $\eta > \bar{\eta}$ can be written as linear combinations of the mode functions $g_\nu(k; \eta)$ and $g_\nu^*(k; \eta)$,

$$S(k; \eta) = A(k)\, g_\nu(k; \eta) + B(k)\, g_\nu^*(k; \eta) \quad , \quad \eta > \bar{\eta} \quad ,$$
(3.27)

where the coefficients $A(k)$ and $B(k)$ can be read from eq.(3.26),

$$A(k) = 1 + i \int_{-\infty}^{0} g_\nu^*(k; \eta) \, \mathcal{V}(\eta) \, S(k; \eta) \, d\eta \tag{3.28}$$

$$B(k) = -i \int_{-\infty}^{0} g_\nu(k; \eta) \, \mathcal{V}(\eta) \, S(k; \eta) \, d\eta \, . \tag{3.29}$$

The coefficients $A(k)$ and $B(k)$ are therefore **calculated** from the **dynamics before** slow roll, that is, during fast-roll. [recall that $\mathcal{V}(\eta) = 0$ for $\eta > \bar{\eta}$ during slow roll.]

The constancy of the Wronskian $W[S(k; \eta), S^*(k; \eta)] = -i$ and eqs. (3.21), (3.27) imply the constraint,

$$|A(k)|^2 - |B(k)|^2 = 1 \quad .$$

This relation permits to represent the coefficients $A(k); \ B(k)$ as [6]

$$A(k) = \sqrt{1 + N(k)} \, e^{i\theta_A(k)} \ ; \ \ B(k) = \sqrt{N(k)} \, e^{i\theta_B(k)} \, , \tag{3.30}$$

where $N(k), \ \theta_{A,B}(k)$ are real.

Starting with Bunch-Davies initial conditions for $\eta \to -\infty$, the action of the fast-roll potential $\mathcal{V}(\eta)$ generates a mixture (Bogoliubov transformation) of the two linearly independent mode functions $g_\nu(k; \eta)$ and $g_\nu^*(k; \eta)$, which result in the mode functions $S(k; \eta)$ eq.(3.27) for $\eta > \bar{\eta}$ when the fast roll potential $\mathcal{V}(\eta)$ vanishes. This is clearly equivalent to starting the evolution of the fluctuations at the *beginning* of slow roll $\eta = \bar{\eta}$ with initial conditions defined by the Bogoliubov coefficients $A(k)$ and $B(k)$ given by eq.(3.29) as stressed in ref. [7].

As shown in ref.[7] the power spectrum of curvature and tensor perturbations for the general fluctuations eq.(3.27) takes the form,

$$P_{\mathcal{R}}(k) \overset{\eta \to 0^-}{=} \frac{k^3}{2\,\pi^2} \left| \frac{S_{\mathcal{R}}(k; \eta)}{z(\eta)} \right|^2 = P_{\mathcal{R}}^{sr}(k) \Big[1 + D_{\mathcal{R}}(k) \Big] \, , \tag{3.31}$$

$$P_T(k) \overset{\eta \to 0^-}{=} \frac{k^3}{2\,\pi^2} \left| \frac{S_T(k; \eta)}{C(\eta)} \right|^2 = P_T^{sr}(k) \Big[1 + D_T(k) \Big] \, .$$

Here $D_{\mathcal{R}}(k)$ and $D_T(k)$ are the transfer functions for the initial conditions of curvature and tensor perturbations introduced in ref.[6]:

$$D(k) = 2 \, |B(k)|^2 - 2 \, \text{Re} \left[A(k) \, B^*(k) \, i^{2\nu - 3} \right] = 2 \, N(k) - 2 \, \sqrt{N(k)[1 + N(k)]} \, \cos \left[\theta_k - \pi \left(\nu - \frac{3}{2} \right) \right] \, . \tag{3.32}$$

where one uses either $_{\mathcal{R}}$ or $_T$ quantities and $\theta_k \equiv \theta_B(k) - \theta_A(k)$.

The standard slow roll power spectra are given by [2]:

$$P_{\mathcal{R}}^{sr}(k) = \left(\frac{k}{2\,k_0} \right)^{n_s - 1} \frac{\Gamma^2(\nu)}{\pi^3} \frac{H^2}{2\,\epsilon_v \, M_{Pl}^2} \equiv \mathcal{A}_{\mathcal{R}}^2 \left(\frac{k}{k_0} \right)^{n_s - 1} \, ,$$

$$P_T^{sr}(k) = \mathcal{A}_T^2 \left(\frac{k}{k_0} \right)^{n_T} \quad , \quad n_T = -2 \, \epsilon_v \quad , \quad \frac{\mathcal{A}_T^2}{\mathcal{A}_{\mathcal{R}}^2} = r = 16 \, \epsilon_v \, . \tag{3.33}$$

These spectra are modified by the fast-roll stage as displayed in eq.(3.31). The scale k_0 is a reference or pivot scale, for example WMAP takes $k_0 = 0.002 \, \text{Mpc}^{-1}$ and CosmoMC, $k_0 = 0.050 \, \text{Mpc}^{-1}$ (see section IV).

The integral equation (3.26) can be solved iteratively in a perturbative expansion if the potential $\mathcal{V}(\eta)$ is small when compared to

$$k^2 - \frac{\nu^2 - 1/4}{\eta^2} \, ,$$

which is indeed true in this case. Then, we can use for the coefficients $A(k), \ B(k)$ the first approximation obtained by replacing $S(k; \eta')$ by $g_\nu(k; \eta')$ in the integrals eqs.(3.28)-(3.29). This is the Born approximation, in which

$$A(k) = 1 + i \int_{-\infty}^{0} \mathcal{V}(\eta) \, |g_\nu(k; \eta)|^2 \, d\eta \quad , \quad B(k) = -i \int_{-\infty}^{0} \mathcal{V}(\eta) \, g_\nu^2(k; \eta) \, d\eta \, . \tag{3.34}$$

The transfer function of initial conditions given by eq.(3.32) can be computed in the Born approximation, which is indeed appropriate in this situation. By using eqs.(3.34) for the Bogoliubov coefficients $A(k)$ and $B(k)$ to dominant order in $1/N$, that is $\nu = 3/2$ [eq.(3.16)], $D(k)$ is given by,

$$D(k) = \frac{1}{k} \int_{-\infty}^{0} d\eta \, \mathcal{V}(\eta) \left[\sin(2\,k\,\eta) \left(1 - \frac{1}{k^2\,\eta^2} \right) + \frac{2}{k\,\eta} \, \cos(2\,k\,\eta) \right] \; . \tag{3.35}$$

The potential $\mathcal{V}(\eta)$ is obtained from eq.(3.15) as

$$\mathcal{V}(\eta) = W(\eta) - \frac{\nu^2 - 1/4}{\eta^2} \; .$$

To explicitly compute $\mathcal{V}_{\mathcal{R}}(\eta)$ as a function of η for the curvature fluctuations we solve numerically the equations of motion (2.7) for new inflation [eq.(2.14)] and insert the solution for the inflaton $\chi(\eta)$ in eqs.(3.9)-(3.10). No large N approximation is used in this numerical calculation since we cover in the evolution the fast-roll region where slow-roll obviously does not apply.

We plot in fig. 2 $\mathcal{V}_{\mathcal{R}}(\eta)$ vs. η for new inflation [eq.(2.14)] for the coupling $y = 1.322$ and a total number of efolds equal to sixty. We choose here the initial values of χ and $\dot{\chi}$ such that their initial kinetic and potential energies are equal. We see that the potential $\mathcal{V}_{\mathcal{R}}(\eta)$ is **attractive** in the fast-roll stage and asymptotically vanishes by the end of fast roll $\eta \sim -0.04$.
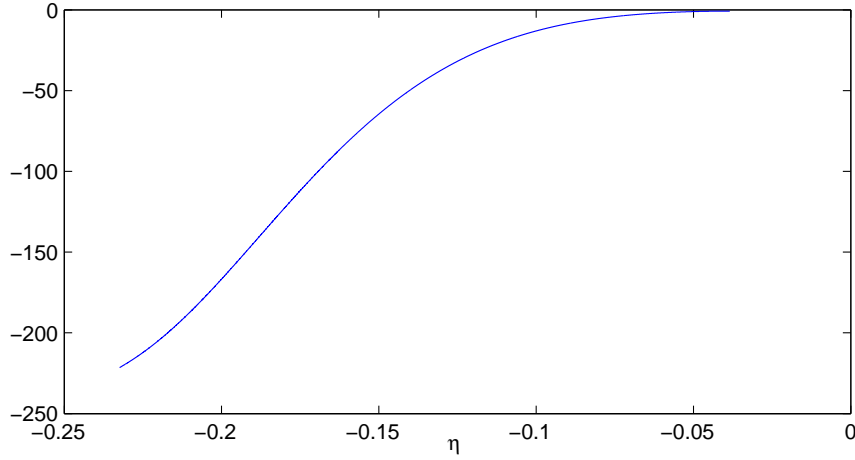

FIG. 2: The potential $\mathcal{V}_{\mathcal{R}}(\eta)$ vs. η for new inflation with $y = 1.322$. $\mathcal{V}_{\mathcal{R}}(\eta)$ is **attractive** during fast-roll and vanishes by the end of fast roll ($\eta \sim -0.04$).

We obtain the transfer function $D_{\mathcal{R}}(k)$ by inserting $\mathcal{V}_{\mathcal{R}}(\eta)$ into eq.(3.35) and computing the integral over η numerically. In fig. 3 we plot $D_{\mathcal{R}}(k)$ vs. k/m for new inflation [eq.(2.14)] and ten different couplings $0.00536 < y < 1.498$ with a total number of efolds equal to sixty. We see that $D_{\mathcal{R}}(k)$ oscillates around zero and therefore produces **suppressions as well as enhancements** in the primordial power spectrum [see eq. (3.31)]. $D_{\mathcal{R}}(k)$ vanishes asymptotically for large k as expected.

The first peak in $D_{\mathcal{R}}(k)$ is clearly its dominant feature. The k of this peak corresponds to k-modes which are today horizon size and affect the lowest CMB multipoles (see below and table 2) [6, 7].

For small k the Born approximation to $D_{\mathcal{R}}(k)$ yields large negative values indicating that this approximation cannot be used in this particular small k regime. We introduce the scale k_1 by the condition $D_{\mathcal{R}}(k_1) = -1$ and then just take $D_{\mathcal{R}}(k) = -1$ for $k \leq k_1$. This corresponds to vanishing primordial power for the lowest values of k [see fig. 3].

¿From fig. 3 we also see that the plots of $D_{\mathcal{R}}(k)$ for different couplings follow from each other almost entirely by changing the scale in the variable k as summarized by eq.(3.36). Indeed, the characteristic scale k_1 plays here a further important role.

Analysing $\mathcal{V}_{\mathcal{R}}(\eta)$ and $D_{\mathcal{R}}(k)$ for different couplings y we find that they **scale** with k_1. Namely,

$$\mathcal{V}_{\mathcal{R}}(\eta) = k_1^2 \, Q(k_1\,\eta) \quad , \quad D_{\mathcal{R}}(k) = \Psi\left(\frac{k}{k_1}\right) \; , \tag{3.36}$$
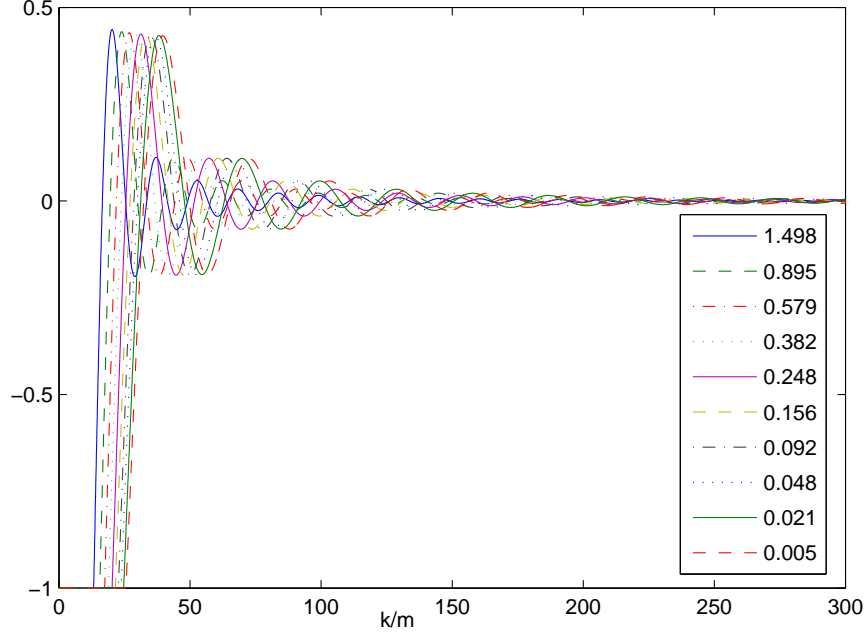
FIG. 3: $D_{\mathcal{R}}(k)$ vs. k/m for new inflation and ten different couplings $0.00536 < y < 1.498$. We see that the plots of $D_{\mathcal{R}}(k)$ for different couplings follow from each other by changing the scale in the variable k as summarized by eq.(3.36).
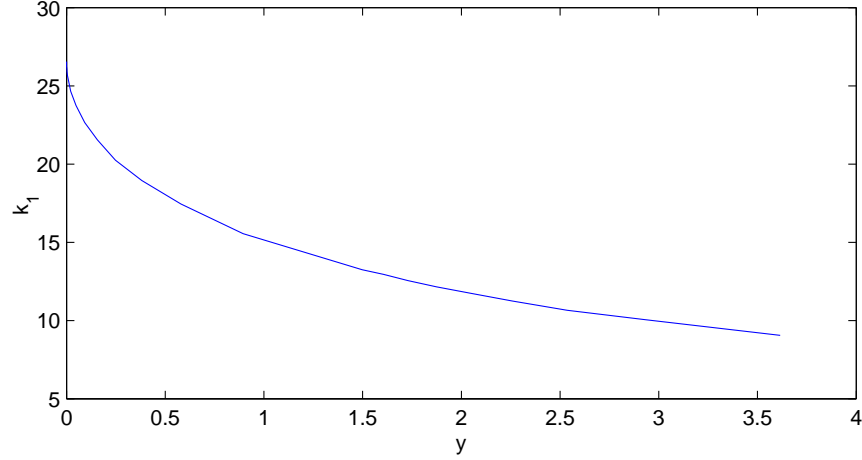

FIG. 4: k_1 vs. y for new inflation.

where $Q(x)$ and $\Psi(x)$ are universal functions. That is, $Q(x)$ and $\Psi(x)$ do not depend on the coupling y while $k_1 = k_1(y)$. We display k_1 vs. y in fig. 4.

We obtain the function $Q(x)$ from eq.(3.36) as,

$$Q(x) = \frac{1}{k_1^2} \, \mathcal{V}_{\mathcal{R}} \left(\frac{x}{k_1} \right) \tag{3.37}$$

We plot $Q(x)$ in fig. 5 as follows from the r. h. s. of eq.(3.37) for ten different values of y. We see that all the curves collapse on a common curve proving the validity of the quasi-scaling properties eq. (3.36).
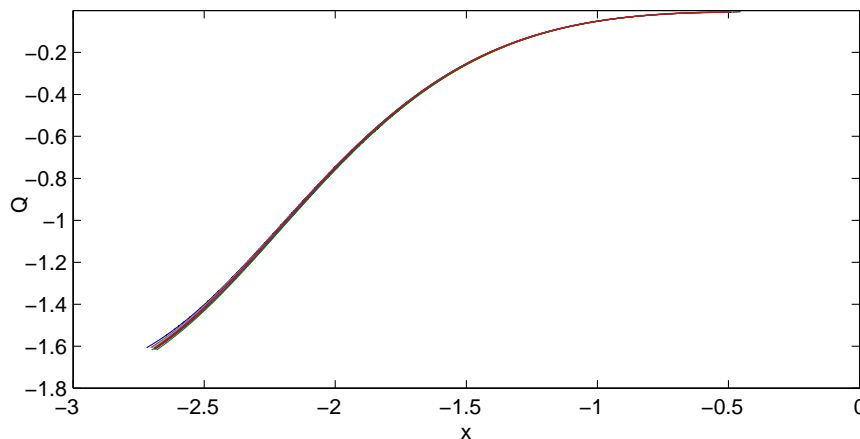
FIG. 5: $Q(x)$ for the ten values of y of fig. 3, according to eq.(3.37). All curves collapse to a common one proving the scaling properties eq. (3.36).

IV.   MCMC ANALYSIS OF CMB AND LSS DATA INCLUDING THE EARLY FAST-ROLL INFLATIONARY STAGE

In order to test the theoretical quadrupole depression predicted by fast-roll inflationary stage against the current experimental data we performed a Monte Carlo Markov Chains (MCMC) analysis of the commonly available CMB and LSS data using the *CosmoMC* program [13].

For LSS we considered SDSS (DR4). For CMB we first considered the three–years WMAP data (with the second release of WMAP likelihood code) and small scale data (ACBAR-2003, CBI2, BOOMERANG03). While this work was in progress the five–years WMAP data were released, and we repeated our MCMC analysis almost completely with these new data, using also the newer 2007 ACBAR release. Actually WMAP-3 or WMAP-5 provide by far the dominant contribution and small scale experiments have very little relevance for the quadruple depression issue.

In all our MCMC runs we have not marginalized over the SZ (Sunayev-Zel'dovich) amplitude and have not included non-linear effects in the evolution of the matter spectrum. The relative corrections are in any case not significant [8, 15], especially in the present context.

CosmoMC is a publicly available open–source FORTRAN package that performs MCMC analysis over the parameter space of the Standard Cosmological model and variations thereof. The main observables in this approach are the correlations among the CMB anisotropies and in particular: the TT (Temperature–Temperature), the TE (Temperature–E_modes), the EE (E_modes–E_modes) and the BB (B_modes–B_modes) correlation multipoles (E_modes and B_modes are special modes of the CMB polarization). These multipoles can be numerically calculated with very good accuracy, as functions of the cosmological parameters, from the primordial power spectrum through programs such as CAMB (included in CosmoMC). On the other side, experimental data provide a likelihood distribution for multipoles, which is then turned into a likelihood for the cosmological parameters through the MCMC method. We modified the *CosmoMC* code introducing the transfer function $D_{\mathcal{R}}(k)$ in the primordial power spectrum according to eq. (3.31).

We ran *CosmoMC* on pc clusters with Message Passing Interface (MPI), producing from 10 to 24 parallel chains, with the 'R-1' stopping criterion (which looks at the fluctuations among parallel chains to decide when to stop the run) set equal to 0.03. The statistical converge was also verified a posteriori with the help of the *getdist* program of *CosmoMC*.

The preferred reference model for slow–roll inflation cosmology is the ΛCDM+r model, that is the standard ΛCDM model, which has six parameters[1], augmented by the tensor-scalar ratio r. Indeed, the current experimental accuracy provides sensible bounds only for the first order parameters ϵ_v and η_v, through their standard relation to the scalar spectral index n_s and the ratio r : $n_s - 1 = 2\eta_v - 6\epsilon_v$, $r = 16\epsilon_v$. Specific slow–roll scenarios, such as those based on

---

[1] we use the standard ones of CosmoMC, that is the baryonic matter fraction ω_b, the dark matter fraction ω_c, the optical depth τ, the ratio of the (approximate) sound horizon to the angular diameter distance θ, the primordial superhorizon power in the curvature perturbation at 0.05 Mpc^{-1}, A_s and the corresponding scalar spectral index n_s

new (small–field) or chaotic (large–field) inflation, connect in a model–dependent way ϵ_v and η_v to free parameters in the inflaton potential and thus typically lead to specific theoretical constraints in the (n_s, r) plane [15].

We point out that we used the default *CosmoMC* pivot scale $k_0 = 0.05$ Mpc^{-1} rather than the customary WMAP choice of $k_0 = 0.002$ Mpc^{-1}. As evident from eq. (3.33) this leads to a small difference with respect to the WMAP choice in the definition itself of the tensor-scalar ratio r. In particular, the CosmoMC r is roughly 10% larger than the WMAP one.

A. MCMC analysis without quadrupole suppression: $D_{\mathcal{R}}(k) = 0$.

Let us present our MCMC analysis with the standard slow-roll primordial power eq.(3.33). That is, without including the early fast roll stage and therefore vanishing transfer function $D_{\mathcal{R}}(k)$.

For instance, in the simplest binomial realization of new inflation described by the inflation potential of eq. (2.12) or eq. (2.14), n_s and r are constrained to the curve C_{BNI} (BNI stands for *Binomial New Inflation*) parametrized by the quartic coupling y as [15]:

$$n_s = 1 - \frac{y}{N}\frac{3z+1}{(1-z)^2} , \qquad r = \frac{16\,y}{N}\frac{z}{(1-z)^2} , \qquad y = z - 1 - \log z , \qquad z = \frac{y}{8}\chi^2 , \qquad 0 < z < 1 . \qquad (4.1)$$

This situation is clearly displayed in fig. 6 in which the curve C_{BNI}, for the two choices $N = 50$ and $N = 60$, is drawn over the contour plot of the likelihood distribution for n_s and r in the ΛCDM+r model obtained with CosmoMC, using the WMAP-3, small-scale CMB and SDSS data. Practically, the same contour plot applies when WMAP-5 and ACBAR-2007 are used.

The likelihood L, as function of the whole set of parameters, provides a quantitative measure of the power of a given model to fit the multipoles C_ℓ^γ. As customary, we set $-2 \log L = \chi_L^2$, although it is well known that, due particularly to cosmic variance, the shape of L, as function of the C_ℓ^γ, is not Gaussian especially for low ℓ.

Now, as evident from eq. (4.1) and fig. 6, one could expect from the ΛCDM model constrained to C_{BNI} a fit to the data not as good as in the ΛCDM+r model since the current data seem to favor smaller values for r. Indeed we find

$$\min \chi_L^2(\Lambda\mathrm{CDM} + r \text{ on } C_{\mathrm{BNI}}) - \min \chi_L^2(\Lambda\mathrm{CDM} + r) \simeq 0.4 . \qquad (4.2)$$

This result was obtained for $N = 50$ by direct minimization of χ_L^2 in the neighbourhood of C_{BNI}, using the data of a large collection of long chain runs (with a grandtotal of almost two million steps) for the ΛCDM+r model with the WMAP-3, small–scale CMB and LSS data. The flat priors on the cosmological parameters were the standard ones of CosmoMC, that is

$$0.005 < \omega_b < 0.1 \quad , \quad 0.01 < \omega_c < 0.99 \quad , \qquad 0.5 < \theta < 10$$
$$0.01 < \tau < 0.8 \quad , \qquad 2.7 < \log(10^{10}A_s) < 4 \quad , \quad 0.5 < n_s < 1.5$$

while for the tensor-scalar ratio we imposed as prior

$$0 < r < 0.35 .$$

We repeated the same analysis with the WMAP-5, ACBAR-2007 and SDSS data, this time setting $N = 60$, with no statistically significant change.

Another approach, that unlike the direct minimization of χ_L^2 over C_{BNI} does take advantage of the explicit analytic parametrizations in eq. (4.1), is to use the single variable z as MCMC parameter, instead of the constrained pair $(n_s\, r)$, with a flat prior over all the allowed range $0 < z < 1$. Let us call $\Lambda\mathrm{CDM}z|C_{\mathrm{BNI}}$ the 6-parameter model ΛCDM constrained on C_{BNI} using the variable z. Then, we find that taking into account the natural fluctuations due to the large number of data (which make the likelihood landscape over the MCMC parametrs quite complex) and the various approximations and numerical errors in the theoretical calculation of the multipoles, the increasing in χ_L^2 due to the C_{BNI} eq. (4.1) constraint compared to the ΛCDM model essentially vanishes [see Table I below].

For completeness and reference, we report in Table I our best fit (or most likely) values for the MCMC cosmological parameters, as well as the absolute value of our best likelihoods, which of course depend on the specific datasets used, that is WMAP-3, small scale CMB and SDSS. We report in the first line of Table I our best fit for the standard ΛCDM model, which has six free parameters since r is set to zero by fiat.

It should be noted that the likelihoods difference between ΛCDM+r and its direct restriction to C_{BNI}, (that is ΛCDM $+r$ on C_{BNI}), is mostly due to the SDSS data, which together with the CMB data place an upper bound
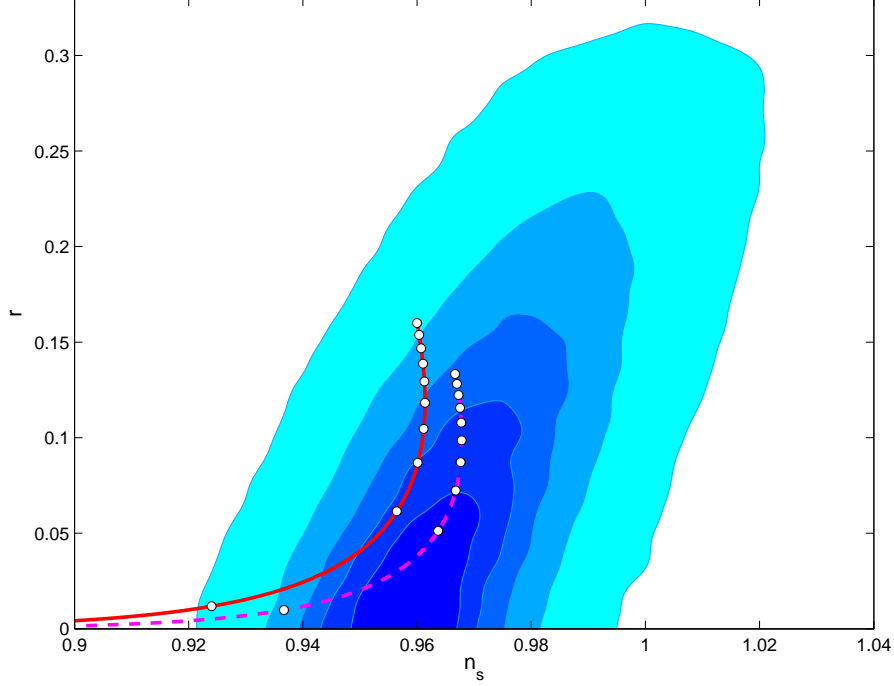
FIG. 6: Binomial New Inflation compared to ΛCDM$+r$ model in the (n_s, r) plane. The color–filled areas correspond to 12%, 27%, 45%, 68% and 95% confidence levels for ΛCDM$+r$ according to WMAP-3, small scale CMB and SDSS data. C_{BNI} is the solid red curve for $N = 50$ or the dashed magenta curve for $N = 60$. The white dots corresponds to the values $0.01 + 0.11 * n$, $n = 0, 1, \ldots, 9$, of the variable z in eq. (4.1), starting from the leftmost ones. The quartic coupling y instead increases monotonically starting from the uppermost dots, which corresponds to the free-field, purely quadratic inflaton potential $y = 0$. We see that very small values of r **are excluded** since they correspond to $n_s < 0.92$ outside the 95% confidence level contour.

	$10\,\omega_b$	ω_c	$10\,\theta$	τ	$10^9 A_s$	n_s	r	$\chi^2_L/2$
ΛCDM	0.224	0.106	1.041	0.886	2.072	0.959	0	2713.906
ΛCDM$+r$	0.224	0.107	1.042	0.831	2.054	0.960	0.009	2713.972
ΛCDM$+r$ on C_{BNI}	0.223	0.106	1.040	0.848	2.047	0.956	0.059	2714.166
ΛCDM$z\vert C_{\mathrm{BNI}}$	0.222	0.107	1.041	0.877	2.065	0.958	0.069	2713.918

TABLE I: Best fit values for the MCMC cosmological parameters without quadrupole suppression, using WMAP-3, small–scale CMB and SDDS. C_{BNI} means the curve on which n_s and r are constrained in Binomial New Inflation (BNI), eq. (4.1) with $N = 50$. ΛCDM$+r$ on C_{BNI} means the ΛCDM$+r$ model constrained on C_{BNI}. ΛCDM$z\vert C_{\mathrm{BNI}}$ denotes the ΛCDM model constrained on C_{BNI} using the single variable z eq. (4.1) as MCMC variable instead of the constrained pair (n_s, r).

on r twice more stringent than WMAP-3 alone. Indeed, when only the WMAP-3 data were used, we verified that no significant likelihoods difference was exhibited. This situation changes slightly when WMAP-5 is used, with χ^2_L increasing approximately by 0.2 from ΛCDM$+r$ to ΛCDM$+r$ on C_{BNI}, since WMAP-5 alone puts a tighter bound on r than WMAP-3 alone (0.43 vs. 0.65 at 95% CL [9]).

It is evident that, as far as most likely values of the cosmological parameters are concerned, the fit with the constraint C_{BNI} included, either with or without z as MCMC parameter, does not determine any statistically significant change, except of course for n_s and r themselves. In particular, with respect to the ΛCDM $+ r$ results, the most likely value of n_s is practically unchanged, while that of r changes from values of order 10^{-2} (or just 0 in ΛCDM) to values such as 0.059 and 0.069 (see Table I).

Concerning marginalized distributions, we find no significant changes but for n_s and r. These results are very close to those in ref. [15], where *trinomial new inflation*, with a possibly asymmetric potential, was considered. In particular, the marginalized distribution for r shows a broad but clear peak centered near the most likely value as in

[15]. In the present context of *binomial* new inflation, we find that $r = 0.089^{+0.044}_{-0.05}$ with $r > 0.023$ at 95% CL.

All together, these results show that, as far as pure data fitting is concerned, the 6-parameter $\Lambda\text{CDM}z|C_{\text{BNI}}$ model is just as good as the standard 6-parameter ΛCDM model. More generally speaking, we may say that current CMB and LSS data together, **without** any theoretical constraint, put only an upper bound on r (namely $r < 0.20$ with 95% confidence level in the most recent WMAP-5 analysis [9]). Therefore, any inflation–based 6-parameter model (as the $\Lambda\text{CDM}z|C_{\text{BNI}}$ model, for instance) predicting a value of r well below 0.2 is as likely as the ΛCDM model itself. This means that the theoretical grounds of a given model take a more important role in the analysis and interpretation of the CMB and LSS data. For instance, from an inflationary viewpoint, the choice that r vanishes exactly appears unlikely and unphysical. Notice that $n_s - 1 = r = 0$ corresponds to a singular and critical (massless) limit where the inflaton potential vanishes [15], while The MCMC analysis for both the binomial and trinomial new inflationary models yield **lower bounds** for r.

In order to asses the statistical relevance of the quadrupole suppression, we determine in the best fit ΛCDM model, the probability that there is at least one multipole, regardless of ℓ, smaller that 20% of the theoretical mean value. We obtained 0.06126 for such probability. Thus, in the ΛCDM, the observed quadrupole realizes a rather unlikely event which has only a 6% probability. Therefore, it makes sense to search for a cosmological explanation of the quadrupole depression beyond the ΛCDM model.

B. MCMC analysis including the quadrupole suppression: $D_{\mathcal{R}}(k) \neq 0$.

Let us now further develop this argument by considering the quadruple depression, avoiding the a priori dismissal based on the simple invocation of cosmic variance or experimental inaccuracy. In the standard ΛCDM model the simplest, purely phenomenological way to decrease the low multipoles is to introduce a infrared sharp cut in the primordial power spectrum of the curvature fluctuations. That is, one assumes that $P_{\mathcal{R}}(k) = 0$ for $k < k_1$ and treats k_1 as a new MCMC parameter to be fitted against the data. It is actually not necessary to include also a cut on the tensor power spectrum, since it would lead to changes certainly not appreciable within the current experimental accuracy.

With this procedure we obtained, using either the WMAP-3 data alone or both CMB and LSS data:

$$\min \chi^2_L(\Lambda\text{CDM} + \text{sharpcut}) - \min \chi^2_L(\Lambda\text{CDM}) \simeq -1.4$$

This result is slightly better than the one reported in ref.[8], but still the likelihood gain hardly compensates the price of a new parameter, especially because its nature appears quite *ad hoc*. In fig. 7 we plot the marginalized probabilities and mean likelihoods of the seven MCMC parameters plus other standard derived parameters in the CMB+LSS case. In the WMAP-3 alone case these plots are almost identical. There are no significant changes from ΛCDM to ΛCDM+sharpcut in their common parameters, in either most likely values or marginalized distributions. The distribution of the new cutoff parameter k_1 shows a well defined peak centered on its most likely value (ML), which corresponds to today's physical wavelength

$$(k_1)_{\text{ML}} = \begin{cases} 0.291 \ (\text{Gpc})^{-1} & (\text{WMAP-3 only}) \\ 0.272 \ (\text{Gpc})^{-1} & (\text{CMB+LSS}) \end{cases} \qquad (\Lambda\text{CDM} + \text{sharpcut}) \ ,$$

that is of the order of today's inverse Hubble radius, as expected.

Introducing the infrared sharp cut on $P_{\mathcal{R}}(k)$ in the $\Lambda\text{CDM}z|C_{\text{BNI}}$ model we find sizably different gains

$$\min \chi^2_L(\Lambda\text{CDM}z|C_{\text{BNI}} + \text{sharpcut}) - \min \chi^2_L(\Lambda\text{CDM}z|C_{\text{BNI}}) = \begin{cases} -1.4 & (\text{WMAP-3 only}) \\ -0.8 & (\text{CMB+LSS}) \end{cases}$$

As before, the difference is due to the tighter bound on r due to the inclusion of the SDSS data. In fact, the most likely values (ML) of k_1 and r corresponding to $\min \chi^2_L(\Lambda\text{CDM}z|C_{\text{BNI}} + \text{sharpcut})$ are given in Table II. The marginalized probabilities in the (r, k_1) plane (converting to a flat prior on r) are shown in the two left panels of fig. 8. There are no significant changes on the other cosmological parameters.

This situation is also reproduced when the fastroll stage is included, that is when the fast roll transfer function $D_{\mathcal{R}}(k)$ eq. (3.35) and fig. 3 is used, treating the scale k_1 in eq. (3.36) as a MCMC parameter.

That is, in the MCMC analysis with fast-roll included, we use the initial power spectrum eq.(3.31) which is modified by the fast-roll transfer function $D_{\mathcal{R}}(k)$. We computed once and forever $D_{\mathcal{R}}(k)$ from eq. (3.35) [see fig. 3]. $D_{\mathcal{R}}(k)$ is a function of k and k_1 with the scaling form eq.(3.36), $\Psi(x)$ being an universal function.
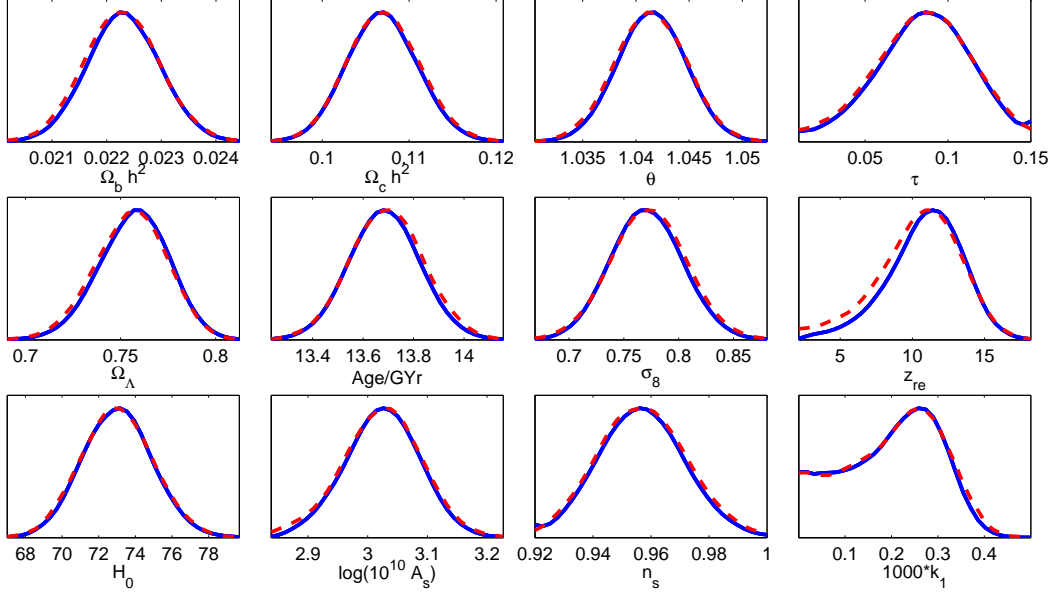
FIG. 7: Marginalized distributions (solid blue lines) and mean likelihoods (red dotted lines) for the parameters of the ΛCDM+sharpcut model.

ΛCDM$z|C_{\mathrm{BNI}}$+sharpcut	k_1 (best fit)	r (best fit)	r (95% CL)
WMAP-3 only	0.275 Gpc^{-1}	0.150	> 0.023
CMB+LSS	0.268 Gpc^{-1}	0.051	> 0.018

TABLE II: The most likely values of k_1 and r and the lower bound on r in the ΛCDM$z|C_{\mathrm{BNI}}$ + sharpcut) model.

We then find

$$\min \chi_L^2(\Lambda\mathrm{CDM}z|C_{\mathrm{BNI}} + \mathrm{fastroll}) - \min \chi_L^2(\Lambda\mathrm{CDM}z|C_{\mathrm{BNI}}) = \begin{cases} -1.8 & (\mathrm{WMAP\text{-}3\ only}) \\ -1.2 & (\mathrm{CMB+LSS}) \end{cases}$$

Correspondingly, in Table III we report the most likely values (ML) of k_1 and r (we report also the best fit for the quartic coupling y for future use) where we used the marginalized probability in the (r, k_1) plane as shown in the two right panels of fig. 8. Here ΛCDM$z|C_{\mathrm{BNI}}$ + fastroll denotes the ΛCDM$z|C_{\mathrm{BNI}}$ model with the fast roll $D_{\mathcal{R}}(k)$ included.

We see a clear peak in y **when** fast-roll or a sharp cut are introduced in the CMB+SDSS fits.

We see that the gains in likelihood are *more significant in the fast-roll case* than in the sharpcut case. Clearly, this fit improvement through power modification by fastroll over power reduction by sharpcut is too small to constitue a real experimental evidence. But still, it is very interesting that the theoretically well founded approach based on fastroll works **better** than the purely phenomenological cutoff. This may be appreciated also from fig. 9 where the best fit for the C_ℓ^{TT} multipoles are compared to the experimental data at low ℓ. We see that the oscillatory form of the fastroll transfer function $D_{\mathcal{R}}(k)$, by **depressing as well as enhancing** the primordial power spectrum at long wavelengths, leads also to new superimposed **oscillatory corrections** on the multipoles. As far as fitting to current data is concerned, such corrections are more effective than the pure reduction caused by a sharp cutoff.

ΛCDM$z|C_{\mathrm{BNI}}$+fastroll	k_1 (best fit)	r (best fit)	r (95% CL)	y (best fit)
WMAP-3 only	0.249 Gpc^{-1}	0.146	> 0.018	0.031
CMB+LSS	0.266 Gpc^{-1}	0.058	> 0.018	1.322

TABLE III: The most likely values of k_1, r and the quartic coupling y and the lower bound on r in the ΛCDM$z|C_{\mathrm{BNI}}$ + fastroll) model.

We did not display in figs. 9 and 10 the ΛCDM+sharpcut results since they are indistinguishable from the BNI+sharpcut values.
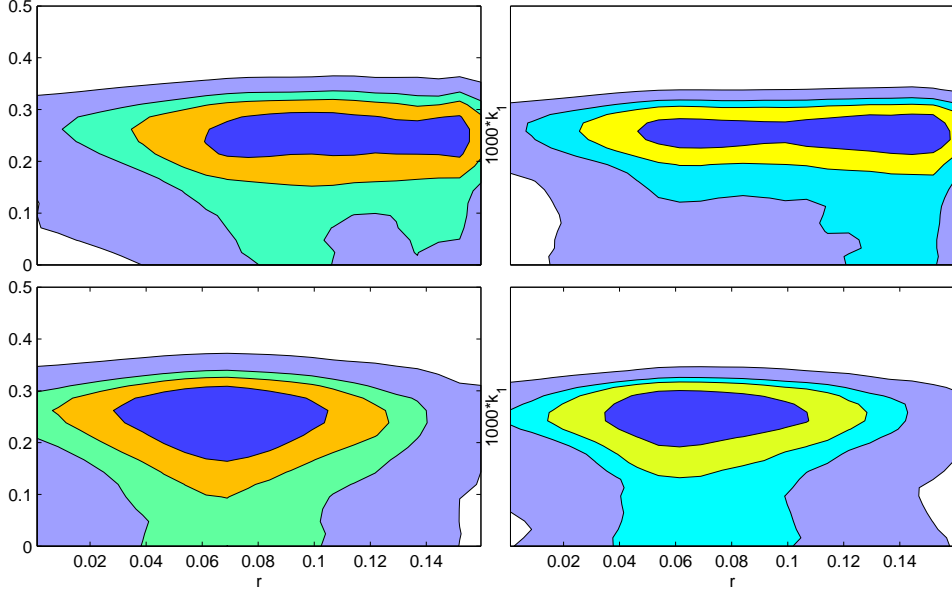

FIG. 8: Marginalized pair distributions in the (r, k_1) plane, at 20%, 41%, 68% and 95% CL, with the WMAP-3 data alone in the top panels and with the CMB+SDSS data in the bottom panels. The left panels refer to the ΛCDM$z|C_{\mathrm{BNI}}$+sharpcut model, while the right ones are for the ΛCDM$z|C_{\mathrm{BNI}}$+fastroll model. k_1 is in Mpc^{-1}.

We plot in fig. 10 the best fit for the C_ℓ^{TE} multipoles compared to the experimental data at low ℓ. We see that for $\ell = 2$ and $\ell = 3$ fast-roll and sharpcut models yield rather similar results (and better than the ΛCDM+r model) while for $\ell = 4$ fast-roll produces a value closer to WMAP-3 data than sharpcut.

We plot in fig. 11 the C_ℓ^{EE} multipoles computed in the best fit point to the WMAP-5 data compared to the experimental WMAP-5 data at low ℓ. We see that both fast-roll and sharpcut models produce a reduction of the low EE multipoles including the EE quadrupole.

Our fits imposing C_{BNI} predict **non-zero** lower bounds on r: at 95% CL, we find that $r > 0.023$ when no cutoff is introduced, while $r > 0.018$ when either the sharp cutoff or the fastroll $D(k)$ are introduced. The best fit values of the other cosmological parameters remain practically unchanged as compared to ΛCDM. Similarly their marginalized probability distributions are almost unchanged, with the natural exception of n_s, which in BNI has a theoretical upper limit [see eq. (5.6)].

C.   Real Space Two Point TT-Correlator

We display in fig. 12 the real space two point TT-correlation function $C^{TT}(\theta)$ for ΛCDM, sharpcut and fast-roll models,

$$C^{TT}(\theta) = \frac{1}{4\pi} \sum_{l=2}^{\infty} (2\,l + 1)\, C_l^{TT}\, P_l(\cos\theta)\ .$$

We see that the ΛCDM correlator becomes really different from the two others only for large angles $\theta \gtrsim 1$. Since all l-modes besides the lowest ones are practically identical in the three cases, this shows how dominant are the low multipoles in the large angle correlations. We also show the WMAP data, the width of the data is mostly due to the cosmic variance.

As is clear from fig. 12, both fast-roll and sharpcut models reproduce the two point correlator $C^{TT}(\theta)$ better than the pure slow-roll ΛCDM+r model.
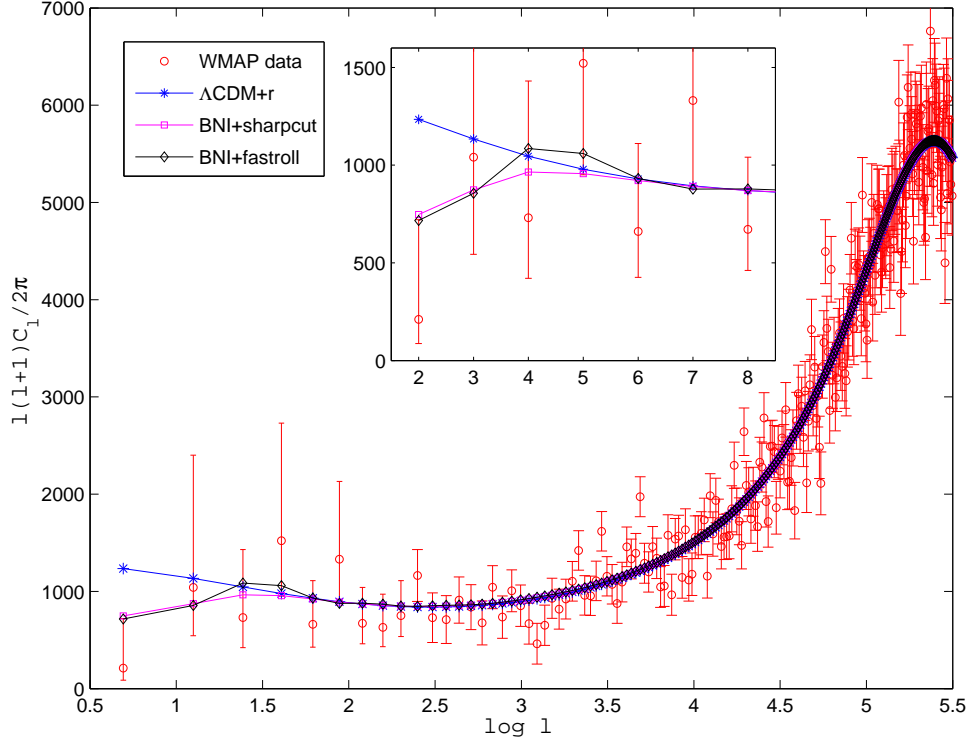
FIG. 9: Comparison, with the experimental WMAP-3 data, of the theoretical C_ℓ^{TT} multipoles computed in the best fit point of the various models of the main text. The error bars in the plotted range of ℓ are mostly due to cosmic variance. The insert contains an enlargement in linear scale of the first seven multipoles. BNI stands for binomial new inflation. The C_ℓ^{TT} units are $[\mu \ K^2]$ and they are plotted as functions of the natural logarithm of ℓ. Error bars of the WMAP-3 data are one-sigma (68%c.l.).

V.   THE TOTAL NUMBER OF E-FOLDS OF INFLATION $N_{tot} = N + 6 \sim 66$

Another interesting observation is possible concerning the number N of efolds since horizon exit till the end of inflation. First of all let us clarify why in all our MCMC runs we keep N fixed. The reason is that the main physics that determines the value of N is **not** contained in the available data but involves the reheating era. Therefore, although technically possible, it is not reliable to fit N solely with the CMB and LSS data within a pure, near scale-invariant slow roll scenario. On the other hand, the quadruple depression allows to set an absolute wavelength scale for the primordial power, so we can check the consistency of our assumptions about N which fixes the total number of efolds of inflation.

In the case of the $\Lambda\mathrm{CDM}z|C_{\mathrm{BNI}}$+fastroll model with the CMB+LSS datasets, the most likely value of the quartic coupling y is slightly larger than unity. Then from fig. 4 we read a value ~ 14 for the ratio k_1/m at horizon exit.

It is important to compare the quadrupole mode scale k_Q with the scale k_1 that characterizes the fast-roll stage.

The physical quadrupole ($l = 2$) wavemodes today k_Q are related to the particle horizon today η_0 by

$$k_Q \ \eta_0 = 3.342 \ldots \ ,$$

where the spherical Bessel function $j_2(k \ \eta_0)$ takes its maximun value, and η_0 is given by [6]

$$\eta_0 = \frac{3.29}{H_0}$$

when one takes into account the acceleration of the universe expansion for $0 < z \lesssim 2$. Therefore, using the present value H_0 [18] we obtain,

$$k_Q = 0.242 \ (\mathrm{Gpc})^{-1} \ .$$

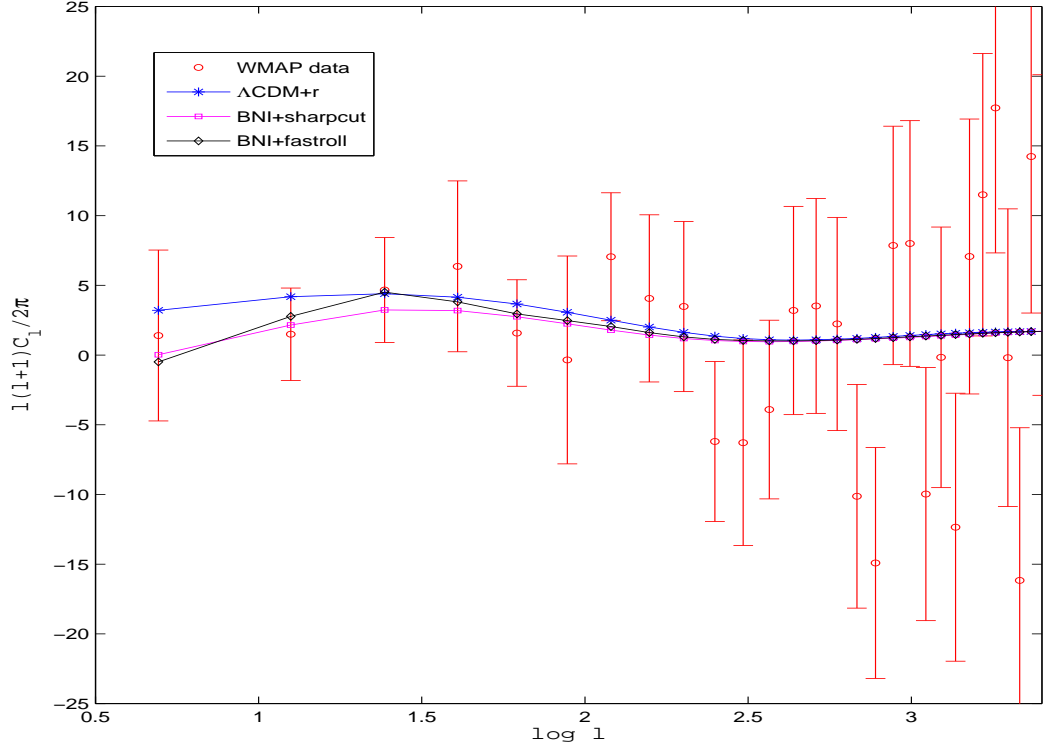Notice that the value of k_Q is **smaller** than the characteristic scale k_1.

FIG. 10: Comparison, with the experimental WMAP-3 data, of the theoretical $C_\ell^{\rm TE}$ multipoles computed in the best fit point of the ΛCDM+r model, fast-roll and sharpcut models. Notice that for $C_2^{\rm TE}$ and $C_3^{\rm TE}$ fast-roll and sharpcut models yield rather similar results (and better than the ΛCDM+r model), while for $\ell = 4$ fast-roll produces a value closer to WMAP-3 than sharpcut. The $C_\ell^{\rm TE}$ units are $[\mu\,K^2]$ and they are plotted as functions of the natural logarithm of ℓ. Error bars of the WMAP-3 data are one-sigma (68%c.l.).

k	$\ln a$ at horizon exit	ϵ_v at horizon exit
$k_Q = 0.242\ {\rm Gpc}^{-1}$	1.01	$0.0276 \gtrsim 1/N$
$k_1 = 0.266\ {\rm Gpc}^{-1}$	1.107	$0.0188 \sim 1/N$
$k_0 = 2\ {\rm Gpc}^{-1}$ (WMAP)	3.135	$\lesssim 1/N$
$k_0 = 50\ {\rm Gpc}^{-1}$ (CosmoMC)	6.363	$\lesssim 1/N$

TABLE IV: The number of efolds since the beginning of inflation when the wavenumbers k_Q, k_1, k_0 exit the horizon. The quadrupole modes **exit** the horizon during the fast roll stage, about $1/10$ of an efold before fast roll ends. k_1 precisely exits the horizon at the **transition** from the fast roll to the slow roll stage.

We display in Table IV the relevant wavenumbers: k_Q, k_1, k_0 and the number of efolds since the beginning of inflation when they exit the horizon. We see that the quadrupole modes **exit** the horizon during the fast-roll stage, approximately $1/10$ of an efold before the end of fast roll. The mode k_1 exit the horizon by $\ln a = 1.107$, very close to the point $\ln a = 1.091$ where $\epsilon_v = 1/N$. That is, k_1 precisely exits the horizon when **fast roll ends and becomes slow roll**.

We denote by k_0 in Table IV the pivot wavenumbers in the WMAP [8] and CosmoMC codes [13], where the indices n_s, r and the running of n_s are computed. Both k_0's exit the horizon well inside the slow roll regime.

We read from Table IV that the **total** number of efolds of inflation is given by

$$N_{tot} = N + 6$$

since we have six efolds before the pivot wavenumber in CosmoMC exit the horizon followed by N efolds of inflation.

We can compute the redshift $1 + z_b$ since the begining of inflation till today comparing $k_Q = 0.242\ ({\rm Gpc})^{-1}$ (today) with $k_Q^{initial} = 0.910\ k_1^{initial} = 12.7\ m$ (at the begining of inflation). [Recall that $1\,{\rm GeV} = 1.564 \times 10^{41}\ ({\rm Gpc})^{-1}$].
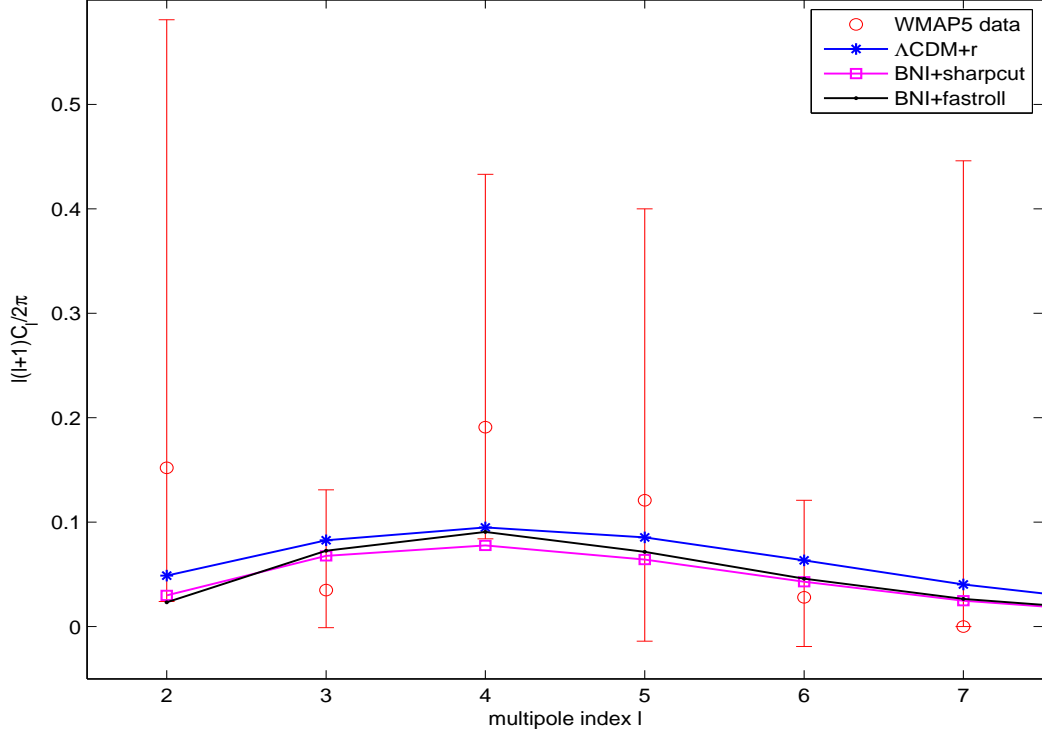
FIG. 11: Comparison, with the experimental WMAP-5 data, of the theoretical C_ℓ^{EE} multipoles computed in the best fit point to the WMAP-5 data of the ΛCDM+r model, fast-roll and sharpcut models as functions of ℓ. Error bars of the WMAP-5 data are one-sigma (68%c.l.). Notice that both fast-roll and sharpcut models produce a depression of the low EE multipoles including the EE quadrupole. The C_ℓ^{EE} units are $[\mu\,K^2]$.

We use for m the value obtained from the scale of inflation [15]

$$ m = \frac{M^2}{M_{Pl}} $$

where M is fixed by the amplitude of the scalar adiabatic fluctuations [8, 15]. We obtain

$$ M = 0.57 \times 10^{16} \text{ GeV} \quad \text{and} \quad m = 1.34 \times 10^{13} \text{ GeV} \quad \text{for} \quad y = 1.322 \,. $$

[Notice that these results are in agreement with the generic estimates eq.(2.4).] Therefore,

$$ 1 + z_b = 1.10 \times 10^{56} \simeq e^{129} \,. $$

Assuming a sharp transition from inflation to radiation dominated expansion, the redshift $1 + z_b$ can be written as

$$ 10^{-56} \sim \frac{1}{1 + z_b} = a_r\, e^{-N_{tot}} \,, \tag{5.1} $$

where a_r is the scale factor at the begining of the radiation dominated era and N_{tot} is the total number of efolds during inflation (during fast-roll plus during slow-roll).

The scale factor at the beginning (a_r) and the end (a_{eq}, equilibration) of the radiation dominated era are related by

$$ \frac{a_{eq}}{a_r} = \sqrt{\frac{H}{H_{eq}}} \,. $$

where H and H_{eq} stand for the Hubble parameter at the beginning and at the end of the radiation dominated era, respectively. For simplicity we assume instantaneous reheating in these formulas.
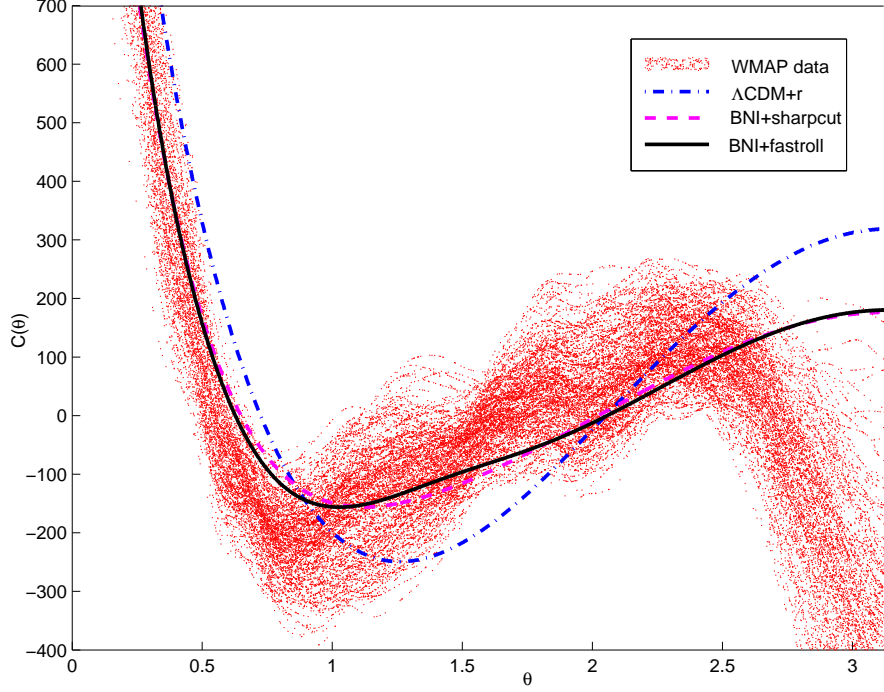
FIG. 12: The real space two point TT correlation function $C^{TT}(\theta)$ for ΛCDM, sharpcut and fast-roll models vs. the angle θ. The ΛCDM correlator differs from the two others only for large angles $\theta \gtrsim 1$. Since all l-modes besides the lowest ones are practically identical in the three cases, this shows how important are the low multipoles in the large angle correlations. Also shown are the WMAP data. The truly observed correlator runs approximately in the middle of the red band. The width of the data band is mostly due to the cosmic variance. The WMAP $C^{TT}(\theta)$ plotted here may not coincide, especially for the largest values $\theta \sim \pi$, with the correlator directly measured from sky maps due to the pixel weighting in the WMAP data analysis. The $C^{TT}(\theta)$ units are $[\mu\,K^2]$.

Furthermore, H_{eq} and H_0 are related by [16]

$$H_{eq} = \sqrt{2\,\Omega_m}\, a_{eq}^{-\frac{3}{2}}\, H_0 \; .$$

where H_0 stands for the Hubble parameter today and Ω_m for the matter fraction of the energy density of the universe today.

Using the current values of the cosmological parameters [18] we find

$$a_r \sim 10^{-29}\, \sqrt{\frac{10^{-4}\, M_{Pl}}{H}} \simeq e^{-67}\, \sqrt{\frac{10^{-4}\, M_{Pl}}{H}} \; . \tag{5.2}$$

Inserting eq.(5.2) into eq.(5.1) yields

$$\frac{H}{10^{14}\text{ GeV}} = e^{2[56-N]} \; . \tag{5.3}$$

Since H must be below its value at the beginning of inflation $\sim 10^{14}$ GeV [see eq.(2.5)], we conclude that

$$N > 56 \; . \tag{5.4}$$

On the other hand, we know from BBN (Big Bang Nucleosynthesis) that H is at least larger than 1 MeV. This together with eq.(5.3) yields the upper bound

$$N < 76 \; . \tag{5.5}$$

Furthermore, our MCMC simulations give good fits for $N \sim 50-60$. The bound eq.(5.4) therefore favours $N \sim 60$ which implies $N_{tot} \sim 66$ and $H \sim 3 \times 10^{10}$ GeV. In addition, from eqs.(5.4) and (5.5) we obtain the bounds $62 < N_{tot} < 82$.

In summary, the fast-roll stage explains the quadrupole suppression and **fixes the total number of efolds** of inflation [6, 7].

Our present MCMC analysis yields $N_{tot} \sim 66$. More generally, the upper bound eq.(5.5) implies $N_{tot} < 82$.

Changing N from 50 to 60 does not affect significatively the MCMC fits we present in this paper. This is partially due to the fact that a change on y can partially compensate a change on N. Another **hint** to increase N above 50 comes from WMAP-5 that gives a larger n_s and using the theoretical upper limit for n_s [14, 15]:

$$n_s < 1 - \frac{1.9236 \ldots}{N} \, , \tag{5.6}$$

which gives $n_s < 0.9679 \ldots$ for $N = 60$. This value is compatible with the n_s value from WMAP5+BAO+SN and no running [9].

Acknowledgments

VI. APPENDIX

As already shown in sec. IV, the four types of correlation multipoles, TT, TE, EE and BB, among the CMB anisotropies can be numerically computed with good accuracy within the CosmoMC program starting from a given cosmological model with a fixed value for all its parameters. To be precise, this computation is performed by the CAMB subprogram, which is an evolution of CMBFAST [17]. CAMB can also compute, with several levels of approximations, the matter power spectrum observable today given the primordial power spectrum of density perturbations.

On modern workstation CPU's, the calculation of two thousand scalar multipoles (related to the primordial curvature fluctuations) and one thousand tensor multipoles (related to primordial gravitational waves) takes less than one second. Thus, within a given type of cosmological model, the theoretical predictions for different choices of parameters can be produced at a very high rate.

To test these predictions against the experimental data CosmoMC makes use of likelihood functions to assign different weights to different sets of correlation multipoles and matter power data. The experimental data and associated numerical code to evaluate such likelihoods is part of CosmoMC in the case of small–scale CMB experiments and LSS surveys. The data and likelihood routines for WMAP are not part of CosmoMC, but they can be downloaded from http://lambda.gsfc.nasa.gov/ and integrated quite easily into CosmoMC, since its interface to CMB likelihoods has been appositely designed for WMAP.

The WMAP likelihood code is particularly complex with respect to the other experiments, due to the wealth of experimental data, the variety of source of systematical errors and the importance of cosmic variance on lower multipoles. Indeed, it has significaly changed and improved along the three WMAP releases. At any rate, it is used in CosmoMC exactly as released by the WMAP team.

Finally, CosmoMC provides the MCMC engine, that is, the routines to perform suitable random walks (the chains) in the parameter space of a give cosmological model in such a way to reconstructs the experimental probability for the parameters from the distribution of values produced along the chains. In our simulations we always employed the default Metropolis rule, where the one-step transition probability from one set λ of parameter values to the next is given by

$$W(\lambda', \lambda) = g(\lambda', \lambda) \min \left\{ 1, \, \frac{L(\lambda') \, g(\lambda', \lambda)}{L(\lambda) \, g(\lambda, \lambda')} \right\}$$

where $g(\lambda', \lambda)$ is a Gaussian proposal, or jump, probability and $L(\lambda)$ is the complete posterior likelihood, that is the product of the prior probability of choosing the starting point of the chain, times the likelihood obtained by comparing the theoretical prediction on multipoles (and matter power if LSS constraints are required) with the experimental data. As is well known from the theory of stationary Markov chains, in the limit of infinitely long chains no dependence is retained on $g(\lambda', \lambda)$ and the reconstructed profile is that of $L(\lambda)$ only. Of course, since actual chains have a finite length, suitable convergence tests are needed to verify that such a reconstruction is accurate enough. On pc-cluster running several parallel chains at once, CosmoMC offers very effective tests of this kind.

In order to test our own models based on Binomial New Inflation, with or without sharp–cut or fast-roll, we needed to modify some routines in CosmoMC. Since our changes with respect to the ΛCDM model are restricted to the primordial power spectrum, only routines relative to the so–called fast variables needed suitable modifications. Fast variables in CosmoMC are cosmological parameters that affect only the primordial spectrum so that, in a Monte Carlo step that proposes changes restricted to them, no need arises to perform the time–consuming recomputation of the transfer functions from a given primordial spectrum to observable multipoles. Slow variables such as the baryonic and dark matter fractions, ω_b, ω_c, the optical depth τ, and the present Hubble parameter H_0 have the opposite definition. No change was done in the by far major portion of the CosmoMC program that deals with slow variables.

We recall also that we let only the four slow variables mentioned above vary in our MCMC run (to be precise, we used the default choice of CosmoMC which replaces H_0 with θ, the ratio of the approximate sound horizon to the angular diameter distance), keeping all other slow cosmological parameters, such as the parameter of the dark energy equation of state or the neutrino density fraction, to the values of the standard ΛCDM model.

[1] Kazanas D, *Astrophys. J.* **241**: L59 (1980); Guth A H, *Phys. Rev.* **D23**, 347 (1981); Sato K, *MNRAS*, **195**: 467 (1981).

[2] See for example: Hu W and Dodelson S, *Ann. Rev. Astron. Ap.* **40**: 171 (2002); Lidsey J, Liddle A, Kolb E, Copeland E, Barreiro T and Abney M, *Rev. of Mod. Phys.* **69**: 373, (1997). Hu W, astro-ph/0402060. Mukhanov VF, Feldman HA and Brandenberger RH, *Phys. Rep.* **215**:203 (1992). A. R. Liddle, D. H. Lyth, *Cosmological Inflation and Large Scale Structure*, Cambridge University Press, 2000; Phys. Rept. **231**, 1 (1993) and references therein.

[3] V. A. Belinsky, L. P. Grishchuk, Ya. B. Zeldovich, I. M. Khalatnikov,
Phys. Lett. **B 155**, 232, (1985), JETP **62**, 195 (1985).

[4] G. F. Smoot *et. al.* (COBE collaboration), Astrophys. J. **396**, 1 (1992).

[5] D. Boyanovsky, H. J. de Vega, N. G. Sanchez, Phys. Rev. **D 73**, 023008 (2006).

[6] D. Boyanovsky, H. J. de Vega, N. G. Sánchez, Phys. Rev. **D 74**, 123006 (2006).

[7] D. Boyanovsky, H. J. de Vega, N. G. Sánchez, Phys. Rev. **D 74**, 123007 (2006).

[8] D. N. Spergel *et. al.* (WMAP collaboration), astro-ph/0603449, Astrophys. J. Suppl., **170**, 377 (2007).

[9] E. Komatsu et al. (WMAP collaboration), arXiv:0803.0547;
G. Hinshaw et al. (WMAP collaboration), arXiv:0803.0732;
M. R. Nolta et al.(WMAP collaboration), arXiv:0803.0593;
J. Dunkley et al. (WMAP collaboration), arXiv:0803.0586.
M. R. Nolta et al.(WMAP collaboration), arXiv:0803.0593.

[10] A. de Oliveira-Costa, M. Tegmark, M. Zaldarriaga and A. J. Hamilton, Phys. Rev. **D69**, 063516 (2004); E. Gaztanaga *et. al.* Mon. Not. Roy. Astron. Soc. **346**, 47 (2003). A. Hajian, astro-ph/0702723. O. Doré et al. Astrophys. J., **612**, 81 (2004). A. Shafieloo, T. Souradeep, Phys.Rev. **D70**, 043523 (2004). A. de Oliveira-Costa and M. Tegmark, Phys.Rev. **D74**, 023005 (2006).

[11] D. Schwarz, G. Starkman, D. Huterer and C. Copi, Phys. Rev. Lett. **93**, 221301 (2004); C. Copi, D. Huterer, D. Schwarz and G. Starkman, Phys. Rev. **D75**, 023507 (2007); A. Rakic, D. Schwarz, Phys. Rev. **D75**, 103002 (2007);

[12] N J Cornish, D N Spergel, G D Starkman, E Komatsu, Phys. Rev. Lett. **92**, 201302 (2004); B F Roukema, B Lew, M Cechowska, A Marecki, S Bajtlik, Astronomy and Astrophysics **423**, 821 (2004); J G Cresswell, A R Liddle, P Mukherjee, A Riazuelo ;Phys. Rev. **D 73**, 041302 (2006); M. Liguori, S Matarrese, M Musso, A Riotto, JCAP **408**, 011 (2004); R. V. Buniy 2005; Int. J. Mod. Phys. **A20**,1095 (2005); R. V. Buniy, A. Berera, T. W. Kephart, Phys. Rev. **D73**, 063529 (2006); T. Multamaki, O. Elgaroy, Astronomy and Astrophysics **423**, 811 (2004); C. Gordon, W. Hu, Phys.Rev. **D70**, 083003 (2004); T. R. Jaffe, A. J. Banday, H. K. Eriksen, K. M. Gorski, F. K. Hansen, Astrophys. J., **629**, L1 (2005); C. Gordon, W. Hu, D. Huterer, T. Crawford, Phys.Rev. **D72**, 103002 (2005); C-H. Wu, K.-W. Ng, W. Lee, D.-S. Lee, Y.-Y. Charng, JCAP **0702**, 006 (2007). L. Campanelli, P. Cea, L. Tedesco, Phys. Rev. Lett. **97**, 131302 (2006), Phys. Rev. **D76**, 063007, (2007). Y. S. Piao, Phys. Rev. **D71**, 087301 (2005). M. Kawasaki, F. Takahashi, Phys. Lett. **B570**, 151 (2003). L. R. Abramo, L. Sodre Jr, C. A. Wuensche, Phys. Rev. **D74**, 083515 (2006). I-C. Wang, K-W. Ng, Phys. Rev. **D 77**, 083501 (2008); J. M. Cline, P. Crotty, J. Lesgourgues, JCAP **0309**, 010, (2003).

[13] A. Lewis, S. Bridle, Phys. Rev. **D66**, 103511 (2002). http://cosmologist.info/cosmomc/

[14] H. J. de Vega, N. G. Sánchez, Phys. Rev. **D74**, 063519 (2006).

[15] C. Destri, H. J. de Vega, N. G. Sánchez, Phys. Rev. **D77**, 043509 (2008).

[16] Kolb EW and Turner MS, *The Early Universe*, Addison Wesley. Redwood City, C.A. 1990.
M. Giovannini, astro-ph/0703730.

[17] Seljak, U., M. Zaldarriaga, Astrophys. J. **469**, 437 (1996).

[18] W.-M. Yao et al., Journal of Physics **G 33**, 1 (2006).